Fermi National Accelerator Laboratory

FERMILAB-PUB-94/164-T
UCLA/94/TEP/3
UVA-INPP-94-01
Pitt-THY-94-08
SHEP-93/94-28
July, 1994

Properties of B-Mesons in Lattice QCD

A. Duncan[1], E. Eichten[2], J. Flynn[3], B. Hill[4], G. Hockney[2], and H. Thacker[5]

[1]Dept. of Physics and Astronomy, Univ. of Pittsburgh, Pittsburgh, PA 15620
[2]Fermilab, P.O. Box 500, Batavia, IL 60510
[3]Physics Dept., Univ. of Southampton, Southampton SO17 1BJ UK
[4]Dept. of Physics, Univ. of California, Los Angeles, CA 90024
[5]Dept.of Physics, University of Virginia, Charlottesville, VA 22901

Abstract

The results of an extensive study of B-meson properties in quenched lattice QCD are presented. The studies are carried out in the static quark limit where the b-quark is taken to be infinitely massive. Our computations rely on a multistate smearing method introduced previously, with smearing functions generated from a relativistic lattice quark model. Systematic errors arising from excited state contamination, finite volume effects, and the chiral extrapolation for the light quarks are estimated. We obtain continuum results for the mass splitting $M_{B_s} - M_{B_u} = 86 \pm 12(stat)\ ^{+7}_{-9}(syst)$ MeV, the ratio of decay constants $f_{B_s}/f_{B_u} = 1.22 \pm 0.04(stat) \pm 0.02(syst)$. For the B-meson decay constant we separately exhibit the sizable uncertainties in the extrapolation to the continuum limit ($a \rightarrow 0$) and higher order perturbative matching. We obtain $f_B = 188 \pm 23(stat) \pm 15(syst)\ ^{+20}_{-0}(extrap) \pm 14(pert)$ MeV.

Operated by Universities Research Association Inc. under contract with the United States Department of Energy

1 Introduction

Heavy-light mesons are ideal systems for lattice QCD studies. For hadrons that contain a single heavy quark, the dynamics of QCD simplifies as $m_Q \rightarrow \infty$. In this limit, the heavy quark is on shell and at rest relative to the hadron[1] and the QCD dynamics becomes independent of m_Q[2]. Heavy quark mass dependence can be extracted analytically to produce an effective action for a static quark and the remaining light degrees of freedom[3, 4]. In the continuum, the resulting heavy quark effective theory (HQET) makes transparent the symmetry[5] and scaling relations between systems which differ by heavy quark spin or flavor [5, 6, 7]. Furthermore for finite heavy quark masses, the effective action can be improved order by order in $1/m_Q$. The $m_Q \rightarrow \infty$ limit may also provide other insights into QCD dynamics. In particular, heavy-light mesons are physical systems with a single light valence quark and fully relativistic QCD dynamics. It is likely that much can be learned about constituent quark ideas in this simple setting[8].

These theoretical developments have immediate physical applications for B physics. Since the b quark mass is significantly heavier than the other mass scales (the QCD scale and the light quarks masses) which enter into the dynamics of B hadrons, it is likely to be a good approximation to treat the b quark in the $m_Q \rightarrow \infty$ limit within B hadrons.

Recent developments in lattice gauge theory have led to the possibility of calculating the masses and decay constants of B_q (q=u, d, s) mesons from first principles (QCD) with enough accuracy to be of both phenomenological and theoretical interest. In particular, we consider the mass difference $M_{B_s} - M_{B_u}$, the decay constant $f_{B_{u,d}}$ and the ratio f_{B_s}/f_{B_d}. We will only consider the lattice action appropriate to the static limit ($m_b \rightarrow \infty$) and hence all the results reported have corrections of order Λ_{QCD}/m_b. A variety of other methods have been developed to study B mesons on the lattice. Methods for treating the b quark using nonrelativistic actions[9], a non-zero velocity formulation[10], and a generalization of the usual Wilson action which is not constrained to quark masses less than the inverse lattice spacing[11] are being actively pursued.

The present study encompasses a systematic analysis of data for M_B and f_B at four different lattice spacings a (with associated beta values $\beta = 5.7, 5.9, 6.1$, and 6.3) and a variety of physical volumes (in lattice units 12^3, 16^3, and 20^3) for one fixed spacing ($\beta = 5.9$). For each case above at least four light quark mass values (kappa values corresponding to pion masses in the range 300 - 800 MeV) were studied. A uniform and consistent fitting scheme was used in all cases. This is particularly important for an accurate extrapolation to results at physical light quark masses ($\kappa = \kappa_{u,d}$ and $\kappa = \kappa_s$). and for assessing the a-dependence of the results.

In the static approximation, the heavy quark propagator is reduced to a straight timelike Wilson line, making it possible to calculate correlators of spatially smeared $\bar{Q}q$ operators without having to compute light quark propagators from smeared sources. Because of this simplifying feature, the heavy-light meson system is an ideal place to develop sophisticated operator smearing techniques. Such techniques are indispensable for the accurate calculation of f_B and other B-meson properties. Until recently, most such calculations have relied on a more-or-less ad hoc choice of smearing functions (e.g. walls[12], cubes [13], or exponentials [14], or Gaussians [14]).

In the present study, we have applied a multistate smearing method introduced previously in Ref. [16]. This analysis provides some significant improvements over previous investigations. First, we have made a serious effort to construct smearing functions which closely resemble the actual Coulomb gauge wave functions of the valence $\bar{Q}q$ system as measured on the lattice. As reported in a previous paper [17], the heavy-light wavefunctions from lattice QCD are reproduced with remarkable accuracy by a simple relativistic quark model (RQM) Hamiltonian which contains the static QCD potential extracted from Wilson lines in Coulomb gauge. In addition to being an interesting statement about QCD dynamics, the success of the RQM has a practical consequence which we will exploit here. The RQM Hamiltonian provides a simple and precise way of constructing orthonormal sets of realistic smearing functions for lattice heavy-light calculations. For each value of β and lattice size. the static Wilson potential is calculated from the gauge configurations and used in the RQM to generate heavy-light smearing functions. The only tuneable parameter in this procedure is the light-quark constituent mass parameter μ in the kinetic term of the RQM Hamiltonian. In practice, this parameter was initially selected by measuring the lattice QCD ground state wavefunction and adjusting μ to give the best fit for the RQM ground state. In some cases, after an initial multistate fit to the heavy-light propagators, it was found useful to iterate the procedure with a more finely tuned value of the constituent quark mass μ, using the more accurate wave functions obtained from the multistate fit.

In addition to this method for constructing smearing functions, another important innovation introduced in the present study is the fitting procedure used to extract information from the heavy-light correlators. Starting with the wavefunctions from the first M S-wave states of the RQM, it is relatively easy to construct the entire $M \times M$ matrix of correlators among the corresponding smeared $\bar{Q}q$ operators, as well as the "smeared-local" correlators between each of these operators and the local $\bar{Q}q$ source. Along with the local-local correlator, these form an $(M+1) \times (M+1)$ matrix. This matrix contains far more information than just the smeared-smeared and smeared-local correlators of any single smearing function. In particular, the matrix contains information about excited states, which, when properly exploited, allows an accurate extraction of ground state properties even at very short time separations, where excited state contributions are still large. The method we introduce to accomplish this employs a χ^2 minimization procedure to simultaneously fit the $(M+1) \times (M+1)$ matrix of correlators to a sum of M exponential (pole) terms, representing the contribution of the M lowest lying heavy-light eigenstates. (In all fits, we exclude the local-local correlator, which, at short time separations, is not well fit by a few low lying states.) The matrix coefficient (residue) of each pole term factorizes and can be written in terms of an $M+1$ component vector whose entries represent the vacuum-to-eigenstate matrix element of each smeared operator. In practice we have found an $M = 2$ fit to yield fairly accurate results for ground state properties. For all of the fits used, the χ^2 per degree of freedom was less than 1.3. The multiparameter fits were carried out using the CERNLIB minimization routine MINUIT.

The improved control over systematic errors gained from the multistate fitting method allows us to better address a number of issues. In particular the dependence of heavy-light meson parameters on both the light quark mass and the lattice spacing are examined in detail. One of the difficulties with previous analyses which prevented accurate chiral and $a \rightarrow 0$ extrapolations was in the arbitrariness of the smearing procedure. It is clear that any ad hoc smearing function will have a substantial overlap with excited states. Typically one tries to optimize the smearing function (e.g. by adjusting the size of the cube) and to go far enough out in time that excited states have died away. The approximate equality of smeared-smeared and smeared-local effective masses, combined with some indication of an effective mass plateau, are the main criteria of success in this procedure. Unfortunately, the procedure is somewhat subjective and it is difficult to rule out large systematic errors due to excited state contamination. An attempt to reduce these errors by extracting results from larger time separations leads to a rapid deterioration of statistics. Moreover, because of the well-known signal-to-noise difficulty for the heavy-light propagator in the static approximation, [15, 16], the problem of isolating the ground state becomes more difficult at smaller lattice spacing. As a result, extrapolation to $a = 0$ is particularly problematic. Furthermore, use of any fixed smearing function at different light quark masses introduces a significant systematic error in the extracted kappa dependence. This is important in the determination of results for f_{B_s}/f_{B_u} and $M_{B_s} - M_{B_u}$. The multistate fitting procedure effectively deals with these difficulties, greatly reducing our errors.

Extrapolating to the continuum limit ($a = 0$) we obtain the ratio $f_{B_s}/f_{B_u} = 1.22 \pm .04(\text{stat}) \pm .02(\text{syst})$ and $M_{B_s} - M_{B_u} = 86 \pm 12(\text{stat})\ ^{+7}_{-9}(\text{syst})\,\text{MeV}$ for the mass difference. For these quantities, only a slight dependence on the lattice spacing is observed, and the systematic errors associated with the $a \to 0$ extrapolation (included in the above) are small.

The situation for the decay constant is more complicated. We find a significant lattice spacing dependence for the ground-state pseudoscalar decay constant f_B. The results for the four β values are consistent with either a linear or quadratic dependence on the lattice spacing a. The linearly extrapolated result in the $a \to 0$ limit is $f_B = 188 \pm 23 \pm 15\,\text{MeV}$ This result is notably smaller than previous estimates of f_B in the static approximation. The primary reason for this is the $a \to 0$ extrapolation. The quadratic extrapolated result in the $a \to 0$ limit is $f_B = 214 \pm 13 \pm 17\,\text{MeV}$. This fit reflects the fact that our results at $\beta = 6.3$ are not inconsistent with those of Ref. [12],[18],[19] (the latter two results using a clover action for the light quarks). In both cases, the first error is statistical while the second includes systematic errors, which we discuss in Section 5. Our final result for the $B_{u,d}$ meson decay constant (in the heavy quark limit) $f_B = 188 \pm 23(\text{stat}) \pm 15(\text{syst})\ ^{+26}_{-0}(\text{extrap}) \pm 14(\text{pert})\,\text{MeV}$ explicitly separates out this theoretical uncertainity associated with the $a \to 0$ extrapolation as well as our estimate of the uncertainity associated with higher order perturbative matching corrections.

We will give a complete discussion of the perturbative matching of lattice to continuum results in Section 2. We include a discussion of the heavy quark mass renormalization in relation to the residual mass parameter ($\bar{\Lambda} = M_B - m_b(\text{quark})$) of HQET. In Section 3 we discuss our analysis procedure. The details of the multistate smearing technique and the construction of the smearing functions from a relativistic quark model (RQM) are presented. In Section 4 the numerical lattice results at each β are presented. The statistical and fitting errors associated with our final physical results are determined. The light meson results used to set light quark masses are contained in Appendix A. The discussion of systematic errors associated with excited state contamination, finite volume, nonzero light quark masses, scale uncertainities, and the extrapolation to zero lattice spacing are all discussed in Section 5. A study of the time evolution of the wavefunctions for heavy-light states is presented in Appendix B. These results provide an independent check that our multistate smearing analysis has removed excited state contamination. In the Section 6 we present our final results, compare them with other recent calculations, and discuss upcoming studies.

2 Perturbative Matching

2.1 Extracting Properties of Heavy-Light Mesons from LQCD

In this section, we will focus on short-distance corrections to the results obtained from lattice QCD. These corrections are common to both traditional techniques for extracting meson properties and to the multistate smearing method employed here. Explanation of the details of the multistate smearing method are deferred to the next section.

The corrections to the matrix elements of time component of the heavy-light axial current, $J_{05}(n)$, are computed by demanding that the ratio of the current renormalized with some continuum regularization scheme and the lattice-regularized current be unity. To be a little more precise, one computes this ratio, Z, using some matrix element, and from then on one multiplies any result obtained using the lattice-regularized current by Z. The states used to determine Z can be chosen for calculational convenience since the ratio is independent of the choice of states. Although there is no choice of states for which the numerator and denominator of the ratio are separately calculable, because the operators only differ at scales on the order of the cutoffs of the two regularizations, and at these scales QCD is perturbative, the ratio can be calculated in perturbation theory.

The procedure is actually slightly more complicated than explained in the preceding paragraph. Because the lattice QCD calculations are done in the heavy quark effective theory (a theory which does not have the same particle content as the full standard model), it is necessary to compute an additional ratio, Z_{cont}. This is the ratio of the axial current renormalized at the scale m_b^* in the standard model to the axial current renormalized at a scale q^* in the heavy quark effective theory.

The calculations of Z and Z_{cont} are the subject of the following two subsections. An analysis of the heavy quark mass renormalization follows thereafter. In the last subsection, we summarize the various constants used in this study.

2.2 Calculation of Z

The ratio Z introduced above was calculated some time ago, but there is substantial uncertainty in these calculations. Tadpole-improved perturbation theory, as formulated by Lepage and Mackenzie [20], promises to reduce these uncertainties below the ten per cent level at one-loop. The application of the tadpole-improvement program to heavy quark effective theory has recently been discussed by Bernard [21], and calculations have been performed by Hernández and Hill [22]. In this subsection we summarize the calculation of Z within the framework of tadpole-improved perturbation theory. Hernández and Hill considered both the zero-separation and unit-separation point-split heavy-light axial currents. We will restrict our attention here to the zero-separation heavy-light current used in our Monte Carlo calculations. We will further restrict our attention to the case of Wilson fermions with $r = 1$. The use of tadpole-improved perturbation theory results in a substantial reduction in our best estimate of the central value and uncertainty for f_B.

The root of the tadpole-improvement program is a nonperturbative renormalization of the basic operators in the lattice action. These redefinitions absorb the large renormalizations arising from lattice tadpole graphs. A related additional part of the Lepage-Mackenzie prescription is the use of a larger perturbative coupling. If one uses β to determine the perturbative coupling, α_{lat}, one-loop perturbative corrections are consistently underestimated. These perturbation theory problems are due to the fact that α_{lat} is a poor choice of expansion parameter. For example at an inverse lattice spacing of 2 GeV, the tadpole-improved expansion parameter is $\alpha_V = 0.16$, which is twice as large as α_{lat}. Lepage and Mackenzie argue that the best way to arrive at α_V is from a non-perturbative lattice determination of a perturbatively calculable quantity, such as the gauge field plaquette expectation value.

Using tadpole-improvement of the Wilson action for quarks on the lattice as a guide, one can perform tadpole-improvement of the heavy quark action, and this has been done in Ref. [21]. Instead of discretizing

$$S = \int d^4x\, b^\dagger \left(i\partial_0 + gA_0\right) b$$

as

$$S = ia^3 \sum\nolimits_n b^\dagger(n) \Big(b(n) - U_0(n-\hat{0})^\dagger b(n-\hat{0}) \Big),$$

it is discretized as

$$S_{tadpole-improved} = ia^3 \sum\nolimits_n b^\dagger(n) \Big(b(n) - \frac{1}{u_0} U_0(n-\hat{0})^\dagger b(n-\hat{0}) \Big),$$

where u_0 is defined as

$$u_0 \equiv \langle \frac{1}{3}\mathrm{Tr} U_{plaq} \rangle^{1/4}.$$

The combination $U_\mu(x)/u_0$ more closely corresponds to the continuum field $(1 + iagA_\mu(x))$, than does $U_\mu(x)$ itself. With the tadpole-improved action, there is an additional factor of

$1/u_0$ for each gauge field link in the product. Thus the Green's function of two heavy-light currents separated by n_0 lattice spacings in the time direction satisfies,

$$[G_B(n_0)]_{tadpole-improved} = \frac{G_B(n_0)}{u_0^{n_0}}.$$

The B meson decay constant f_B is usually extracted from numerical simulations by fitting $G_B(n_0)$ to

$$\frac{(f_B m_B)^2}{2m_B} \exp[-Cn_0 a]$$

Thus we see that the tadpole improvement procedure has no effect on the fitted value of f_B. Its only effect is the change

$$C \to C + \frac{\ln u_0}{a},$$

that is, a linearly divergent mass renormalization.

So far we have seen that tadpole improvement does not affect the extraction of f_B as it is generally done in lattice Monte Carlo calculations. However we must still take into account the effect of tadpole improvement of the light quark action, and this will involve some additional factors.

As conventionally defined in lattice Monte Carlo calculations the lattice operator J_5^0 involved in calculating f_B is renormalized by a factor $\sqrt{2\kappa_C}Z$, where κ_C is the critical value of the hopping parameter for the light quarks. The tree level value of κ_C is 1/8. Lepage and Mackenzie advocate a reorganization of perturbation theory such that a factor of $\sqrt{8\kappa_C}$ is included in $\tilde{Z}$ and the renormalizing factor becomes $\tilde{Z}/2$.

Let us see what this factor does at one-loop. Calculations of Z have been carried out to one-loop order and the result is of the form,

$$Z = 1 + \frac{\alpha_S}{3\pi}[\int \frac{d^4q}{\pi^2} g(q) + \frac{3}{2}\ln(q^* a)^2].$$

This definition of $g(q)$ (and similar ones for $h(q), j(q)$, and $k(q)$ which will be introduced below) follow the definitions in Ref. [22]. A one-loop calculation of $8\kappa_C$ has been performed, and the result is expressible as

$$\frac{1}{8\kappa_{c,\text{one-loop}}} = 1 - \frac{\alpha_S}{3\pi}\int \frac{d^4q}{\pi^2} h(q).$$

The relationship between $\tilde{Z}$ and Z is

$$\tilde{Z} = \sqrt{8\kappa_{c,\text{one-loop}}}Z.$$

The one-loop expression for $\tilde{Z}$ is therefore

$$\tilde{g}(q) = g(q) + h(q)/2,$$

where

$$\tilde{Z} = 1 + \frac{\alpha_S}{3\pi}\Big[\int \frac{d^4q}{\pi^2}\tilde{g}(q) + \frac{3}{2}\ln(q^*a)^2\Big]$$

We continue with the application of the Lepage-Mackenzie prescription to determine the Λ-value of the coupling and the scale q^* at which it is evaluated. The prescription for fixing the value of the coupling, α_V is to extract it from a non-perturbative calculation of the 1×1 Wilson loop (*i.e.*, the expectation value of the plaquette, U_{plaq}). Once the coupling is known at some scale (alternatively, once the value Λ_V is known), it can be run to any other scale. The formula which relates α_V to the non-perturbatively determined (lattice Monte Carlo) plaquette expectation value is,

$$-\ln\langle\frac{1}{3}\mathrm{Tr}U_{plaq}\rangle = \frac{4\pi}{3}\alpha_V(3.41/a)\left[1 - \alpha_V(3.41/a)(1.19 + 0.025n_f) + O(\alpha_V^2)\right].$$

The coefficient of n_f is the one appropriate for Wilson fermions with $r = 1$. In the quenched approximation, $n_f = 0$. Λ_V is determined through

$$\alpha_V(q) = \left[\beta_0\ln(q^2/\Lambda_V^2) + (\beta_1/\beta_0)\ln\ln(q^2/\Lambda_V^2))\right]^{-1}.$$

It remains to fix the scale q^* at which $\alpha_V(q)$ is evaluated in the expression for $\tilde{Z}$. Lepage and Mackenzie propose to do that by calculating the expectation value of $\ln q^2$ in the one-loop perturbative lattice correction. The formulae determining this scale are:

$$\begin{aligned} Y &\equiv \int d^4q\ \tilde{g}(q) = -13.93 && (1)\\ \langle\ln(qa)^2\rangle &\equiv \frac{1}{Y}\int d^4q\ \tilde{g}(q)\ln(q^2a^2) = \frac{21.76}{13.93} && (2)\\ q^*a &\equiv \exp[\langle\ln(qa)^2\rangle/2] = 2.18\ . && (3) \end{aligned}$$

Hernandez and Hill quote the errors on the numerically evaluated values of Y and $Y\ln < q^2 >$ as order 1 in the last decimal place.

Using the two-loop formula for the running of α_V with zero quark flavors one obtains $\alpha_V(q^*)$. The explicit dependence on the value of a^{-1} drops out of the ratio q^*/Λ_V. Hence, the only way lattice Monte Carlo results have been used so far is for the expectation value of the plaquette; the determination of a^{-1} has not yet entered. The results for Z at various values of β are summarized in Table 1.

This completes our calculation of $\tilde{Z}$. It remains to multiply $\tilde{Z}$ by the continuum running and matching factor, Z_{cont}. We leave this for the following subsection.

2.3 Continuum Running and Matching Factor

For consistency, the one loop computation of $\tilde{Z}$ should be combined with a two loop running in the continuum effective theory and a further one loop matching between the continuum effective and full theories. This produces the continuum running and matching factor Z_{cont} which multiplies $\tilde{Z}$ to give the full perturbative correction. It will turn out that the lattice to continuum matching factor $\tilde{Z}$ is most significant, while Z_{cont} produces only a small additional change.

In the previous section, the coupling α_V was determined in a no-flavor (quenched) lattice theory. We must now match onto a four-flavor (or five-flavor depending on the value of q^*) continuum theory. In order for the infrared behavior of lattice and continuum theories to match exactly, we could use a continuum coupling whose value is equal to $\alpha_V(q^*)$ (although differences between couplings are higher order effects). This implies we should choose a continuum scale q_{cont} according to $\alpha_{cont}(q_{cont}) = \alpha_V(q^*)$. In practice we ignore this criterion and simply set $q_{cont} = q^*$, using $\alpha_V(q^*)$ everywhere in the matching. We then run in the continuum theory using four or five flavors depending on whether q^* is greater or less than the b-quark threshold mass.

The b-quark threshold itself is determined as follows. We assume the pole mass $m_{b\,pole}$ is known and relate it to the $\overline{\text{MS}}$ running mass $m_b(\mu)$ according to [23]

$$m_{b\,pole} = m_b(\mu)\left(1 + \frac{\alpha_{cont}(\mu)}{\pi}\left[\frac{4}{3} + \ln(\mu^2/m_b^2(\mu))\right]\right).$$

Setting $\mu = m_b^* = m_b(m_b^*)$, we fix the threshold mass m_b^* by solving

$$m_{b\,pole} = m_b(m_b^*)\left[1 + \frac{4\alpha_{cont}(m_b^*)}{3\pi}\right]$$

We use the usual two loop result for α_{cont}:

$$\alpha_{cont} = \frac{4\pi}{b_0\ln(\mu^2/\Lambda^2)}\left(1 - \frac{b_1\ln\ln(\mu^2/\Lambda^2)}{b_0\ln(\mu^2/\Lambda^2)}\right)$$

with

$$b_0 = 11 - 2n_f/3, \qquad b_1 = 102 - 38n_f/3.$$

Here n_f is the number of light flavors and we take $\Lambda = 175\,\mathrm{MeV}$ for five light flavors [24]. For other n_f, Λ is fixed by demanding that α_{cont} be continuous. Applying this procedure with $m_{b\,pole} = 4.72\,\mathrm{GeV}$ [25] gives

$$m_b^* = 4.34\,\mathrm{GeV}.$$

Now that q^* and m_b^* are fixed we use them in the combined two loop running plus one loop matching formula for Z_{cont}. The one-loop anomalous dimension calculation [26] for the heavy-light axial current was extended to two loops by Ji and Musolf [27] and the two loop result was confirmed by Broadhurst and Grozin [29]. The same authors [30] also confirmed the one-loop matching calculation of Eichten and Hill [31]. The result for Z_{cont} is:

$$\begin{aligned} Z_{cont} \quad = \quad & \left(\frac{\alpha_{cont}(m_b^*)}{\alpha_{cont}(q^*)}\right)^{\gamma_0/2b_0} \times \\ & \left(1 + \frac{\alpha_{cont}(m_b^*) - \alpha_{cont}(q^*)}{4\pi}\left[\frac{\gamma_0}{2b_0}\left\{\frac{\gamma_1}{\gamma_0} - \frac{b_1}{b_0}\right\}\right] + \frac{c_1\alpha_{cont}(m_b^*)}{4\pi}\right). \end{aligned} \tag{4}$$

In this equation γ_0 and γ_1 come from the anomalous dimension γ of the heavy-light axial current in the effective theory,

$$\gamma = \gamma_0\frac{\alpha_{cont}}{4\pi} + \gamma_1\left(\frac{\alpha_{cont}}{4\pi}\right)^2,$$

while c_1 comes from the effective to full theory matching at one loop in the continuum, obtained by the method described at the beginning of section 2.1. This matching produces a contribution to Z_{cont} of

$$1 + c_1\frac{\alpha_{cont}}{4\pi}.$$

Note that Ji and Musolf [27] quote c_1 with a sign error in the term which differs for vector and axial vector currents. The values of γ_i and c_1 are:

$$\begin{aligned} \gamma_0 &= -4 \\ \gamma_1 &= -254/9 - 56\pi^2/27 + 20n_f/9 \\ c_1 &= -8/3 \end{aligned}$$

Using equation (4) we determine the Z_{cont} values given in Table 1. These are then combined with the $\tilde{Z}$'s obtained in the previous subsection to give the overall perturbative

Table 1: Length scales and renormalization constants used in this paper. The values of a^{-1} for $\underline{=}5.7, 5.9$, and 6.1 are taken from Ref. [43]. For $\beta = 6.3, a^{-1}$ is estimated from that at 6.1 by one-loop asymptotic freedom. Plaquette expectation values are taken from [20]. $\tilde{Z}$ is the lattice to continuum renormalization factor for the axial current, Z_{cont} is the factor relating the continuum heavy quark effective theory to full QCD, and Z_A is the overall renormalization factor used in previous discussions.

β	a^{-1}(GeV)	$\langle \frac{1}{3}\mathrm{Tr}\, U_{\mathrm{plaq}} \rangle$	$\tilde{Z}$	Z_{cont}	Z_A
5.7	1.15(8)	0.549	0.73	1.00	.63
5.9	1.78(9)	0.582	0.77	0.96	.65
6.1	2.43(15)	0.605	0.80	0.94	.68
6.3	3.08(18)	0.623	0.81	0.93	.68

corrections Z listed in Table 1. Here, to conform with our previous notation [28] we also list the quantity

$$Z_A = \frac{\tilde{Z} Z_{cont}}{\sqrt{8\kappa_c}} \tag{5}$$

2.4 Renormalization of the Heavy Quark Mass

Before leaving the subject of short-distance perturbative correction we will compute the tadpole-improved estimate of heavy quark mass renormalization.

In the continuum static limit neither the heavy meson mass (M_B) nor the renormalized heavy quark mass (m_b) appears explicitly, only the residual mass combination $\bar{\Lambda} = M_B - m_b$ remains. The precise definition of the renormalized mass parameter in the dimensionally regularized heavy quark effective theory has been discussed by Falk, Neubert, and Luke [32]. Since the heavy quark mass renormalization is a linear divergence it vanishes in dimensional regularization with minimal subtraction.

On the lattice, the heavy quark mass is renormalized in the static limit. This mass shift, δm, is proportional to $1/a$ with a perturbatively calculable coefficient. Hence the mass, M_{eff}, calculated for the ground state B meson in this lattice theory can be expressed as

$$M_{eff} = \bar{\Lambda} - \delta m; \tag{6}$$

in terms the continuum residual mass $\bar{\Lambda}$ and the mass shift δm. It is clear from Eq.(6) that the mass M_{eff} is linearly divergent as the lattice spacing $a \to 0$. However, it would appear that by measuring M_{eff} and removing the tadpole-improved one-loop mass counterterm, we have a determination of $\bar{\Lambda}$. Hence we could obtain m_b as defined in Ref. [32] from m_B. Unfortunately, Bigi *et al* [33] argue that non-perturbative effects ruin the preceding connection. Even if that is so, it is still possible to verify that the linearly divergent piece of M_{eff} is correctly determined by the perturbative calculation of δm.

At one loop, the lattice heavy quark mass renormalization is of the form,

$$\delta m = -\frac{\alpha_S}{3\pi}\frac{1}{a}\int \frac{d^4q}{\pi^2}k(q) \; .$$

The one-loop correction to the self-energy is linearly divergent and positive. The coefficient, δm, of the mass counterterm is negative. The integrand k(q) is given by [34],

$$k(q) = \frac{1}{8}\left[\sum_{\alpha=1}^{3}\sin^2(q_\alpha/2)\right]^{-1} \; .$$

As already noted the effect of tadpole improvement on the fitted value of the heavy quark mass is to change

$$C \rightarrow C + \frac{\ln u_0}{a},$$

This non-perturbative reduction of the mass is accompanied by a reduction in the counterterm:

$$\widetilde{\delta m} = -\frac{\alpha_S}{3\pi}\frac{1}{a}\int \frac{d^4q}{\pi^2}\tilde{k}(q) \; .$$

where

$$\tilde{k}(q) = k(q) + j(q)$$

As in the calculation of the scale q^*, we need to compute the expectation vlaue of $\ln q^2$ in the integral of $\tilde{k}(q)$. The formulae determining this scale are:

$$X \equiv \int d^4q \; \tilde{k}(q) = 10.07 \qquad (7)$$

$$\langle \ln(qa)^2 \rangle \equiv \frac{1}{X}\int d^4q \; \tilde{k}(q)\ln(q^2a^2) = \frac{14.34}{10.07} \qquad (8)$$

$$p^*a \equiv \exp[\langle \ln(qa)^2 \rangle/2] = 2.04 \; . \qquad (9)$$

The calculational technique used is exactly that of Ref. [22], and the errors on the numerically evaluated values of X and $X\ln < q^2 >$ are order 1 in the last decimal place.

The values of $\alpha_V(p^*)$ at the β values used in this study and $a\widetilde{\delta m} + \ln u_0$ are presented in Table 2.

Table 2: Tadpole improved mass counterterm for a static quark at the β values used in this paper. The associated gauge couplings $\alpha_V(p^*)$ are also listed. The scale p^* is $2.04/a$ (see text).

β	$\alpha_V(p^*)$	$a\widetilde{\delta m} + \ln u_0$
5.7	0.228	-0.394
5.9	0.191	-0.339
6.1	0.170	-0.307
6.3	0.156	-0.285

Two methods for the determination of $\bar{\Lambda}$ are possible. The first of these is to do the tadpole-improved perturbative subtraction just described. This results in a statistically independent result for $\bar{\Lambda}$ for each β value. The second method is to use the fact that the subtracted term is proportional to $1/a$, and the physical value desired is independent of the lattice spacing. A two-parameter fit of the mass over the four values of β has two degrees of freedom, and one of the parameters is the one we desire. The latter procedure ignores the running of the coefficient of the 1/a term.

2.5 Comparison and Summary

It is worthwhile at this point to compare the results in Table 1 with the widely used value of Z_A of 0.8, which does not benefit from tadpole improvement. Consider the results at $\beta = 6.1$. From the table, we find $\tilde{Z}Z_{cont}/\sqrt{8\kappa_c}$ to be 0.68. Consequently, tadpole-improved perturbation theory results in a reduction of the physical value of f_B by a factor of 0.68/0.8, *i.e.*, a reduction of 18%.

As an aside, we note that for the clover action—also termed "improved", but in the sense that order a effects rather than tadpole graphs are being incorporated—the axial current has been renormalized [35], but tadpole improvement has not been applied to this operator.

Now that perturbation theory has been reorganized to include tadpole corrections to all orders, we expect our one-loop calculation of the renormalization factor to be accurate to about 7%. This estimate of the magnitude of the two-loop corrections is obtained simply by squaring the largest one-loop correction for the various values of r quoted in Ref. [22], for both discretizations of the axial current considered there.

While the values for Z_{cont} depend on the estimate of the lattice spacing, this dependence is weak; an increase by 10% in the estimate of the scale results in a reduction of at most 1.5% in the value of Z_{cont}. Thus this source of uncertainty in the Z factor is negligible compared to both the estimated size of the two-loop corrections or the direct dependence of f_B on the lattice spacing.

3 Analysis Procedure for Multistate Smearing

3.1 Relativistic Quark Model for Heavy-light Systems

The rapid deterioration[15, 16] of the signal to noise quality of Euclidean correlators of heavy-light mesons at large Euclidean time makes the choice of an efficient smearing scheme essential if we wish to extract accurately the properties of low-lying heavy-light systems. In the multistate smearing approach previously introduced[16], the coupling of smeared bilocal Coulomb gauge operators to higher meson states was reduced by using smearing wavefunctions obtained from a relativistic quark model (RQM). The basic features of such a model are (a detailed examination of the connection of such a model with the full field theory in the case of the t'Hooft model can be found in [36];see also,[37]):

(a) the use of a relativistic kinetic term $\sqrt{p^2+\mu^2}$ (with μ a constituent quark mass) for the kinetic piece of the Hamiltonian, and

(b) a static confining potential $V(\vec{r})$, which can be chosen to be the static interaction energy obtained from correlators of temporal Wilson lines in lattice QCD.

The importance of relativistic kinematics in determining the shape of meson wavefunctions (with a light quark) was already implicit, if not clearly recognized, in the puzzling persistence of purely exponential falloff ($\simeq \exp -Cr$) of hadronic wavefunctions, instead of the more rapid falloff one might naively expect in a confining model ($\simeq \exp -Cr^{3/2}$ for a nonrelativistic particle in a linearly rising potential). This exponential falloff is due to the nonlocal character of the kinetic part of the RQM Hamiltonian

$$\begin{aligned} K(\mid r-r'\mid) &\equiv \int \sqrt{p^2+\mu^2}\exp i\vec{p}\cdot(\vec{r}-\vec{r}')d^3p &(10)\\ &\simeq \mid r-r'\mid^{-9/2}\; e^{-\mu|r-r'|}, \quad \mid r-r'\mid\to\infty &(11)\end{aligned}$$

which implies that $\Psi_n(r)$ satisfying

$$\int d^3r' K(\mid r-r'\mid)\Psi_n(r') + V(r)\Psi_n(r) = E_n\Psi_n(r) \tag{12}$$

cannot fall exponentially faster than $e^{-\mu r}$ (if it did, the integral over r' in (12) would be dominated by $r'\simeq 0$, giving an asymptotic behavior $\simeq e^{-\mu r}$ for the kinetic term, in contradiction with the assumed asymptotic behavior of $(E_n - V(r))\Psi(r)$ for *any* $V(r)$ with power growth). In other words, irrespective of the power rise of the confining potential, relativistic kinematics automatically smears out the wavefunction of a light quark over the Compton wavelength corresponding to the constituent quark mass.

In the static limit in which the heavy quark mass is taken to infinity, the relativistic Schrodinger equation (12) gives a single parameter fit (the constituent quark mass μ is the only adjustable parameter after the static potential has been measured on the lattice) to a complete set of orthogonal spin-independent wavefunctions corresponding to arbitrary radial and orbital excitations of the heavy-light system. To minimize lattice discretization and finite volume artifacts in the comparison of RQM and lattice Monte Carlo results, we have generated a set of lattice smearing functions by solving a discretized version of (12), in each case on lattices of the same size as those used in the Monte Carlos, and in each case with the static potential determined from Wilson line correlators in the same gauge configurations used to extract our quenched QCD results. Namely, on each lattice and for each β value, we have extracted a full lattice static potential $V(\vec{r})$ by measuring the correlator of two Wilson lines of time extent T (in Coulomb gauge-fixed configurations), and separated by a spatial distance $\vec{r}$. The potential is then extracted by going out in Euclidean time T until the static energy $\mathcal{E} = -\frac{1}{T}\ln < W(0,T)W^{\dagger}(\vec{r},T) > \equiv V(\vec{r})$ stabilizes (for example, with β =5.9 on a 16^3 lattice, this occurs for $T \geq 5$). The static potential extracted at various β values and lattice sizes is displayed in Fig[1].

The procedure used for generating lattice smearing functions from the RQM is as follows. We wish to obtain orthonormal lattice wavefunctions which are eigenstates of a lattice RQM Hamiltonian defined on a L^3 lattice (with $\vec{r}, \vec{r}'$ lattice sites):

$$H_{\vec{r}\vec{r}'} \equiv K_{\vec{r}\vec{r}'} + V(\vec{r})\delta_{\vec{r}\vec{r}'} \tag{13}$$

$$K_{\vec{r}\vec{r}'} = \frac{1}{L^3}\sum_{\vec{p}}\sqrt{4\sum_i \sin^2\left(\frac{\pi p_i}{L}\right) + \mu^2}\ e^{i\vec{p}\cdot(\vec{r}-\vec{r}')} \tag{14}$$

Such an eigenstate, in a channel of given orbital quantum number (S,P,D etc), will correspond to a pole of the resolvent applied to a source wavefunction $\Psi^{(0)}$ of the same orbital symmetry:

$$R \equiv \|\sum_{r'}\left(\frac{1}{E-H}\right)_{\vec{r}\vec{r}'}\Psi^{(0)}(\vec{r}')\| \to \infty \tag{15}$$

For the starting source functions $\Psi^{(0)}$, one may take for example a monopole localized at the origin for S-states, a dipole for P-states, etc. After the energy E is tuned close to an eigenvalue E_n (until R is at least 10^3 larger than the background value), a smearing eigenstate $\Psi^{(a)}_{\mathrm{smear}}(\vec{r})$ is extracted by renormalizing the vector $\frac{1}{E-H}\Psi^{(0)}$ to unit norm. The

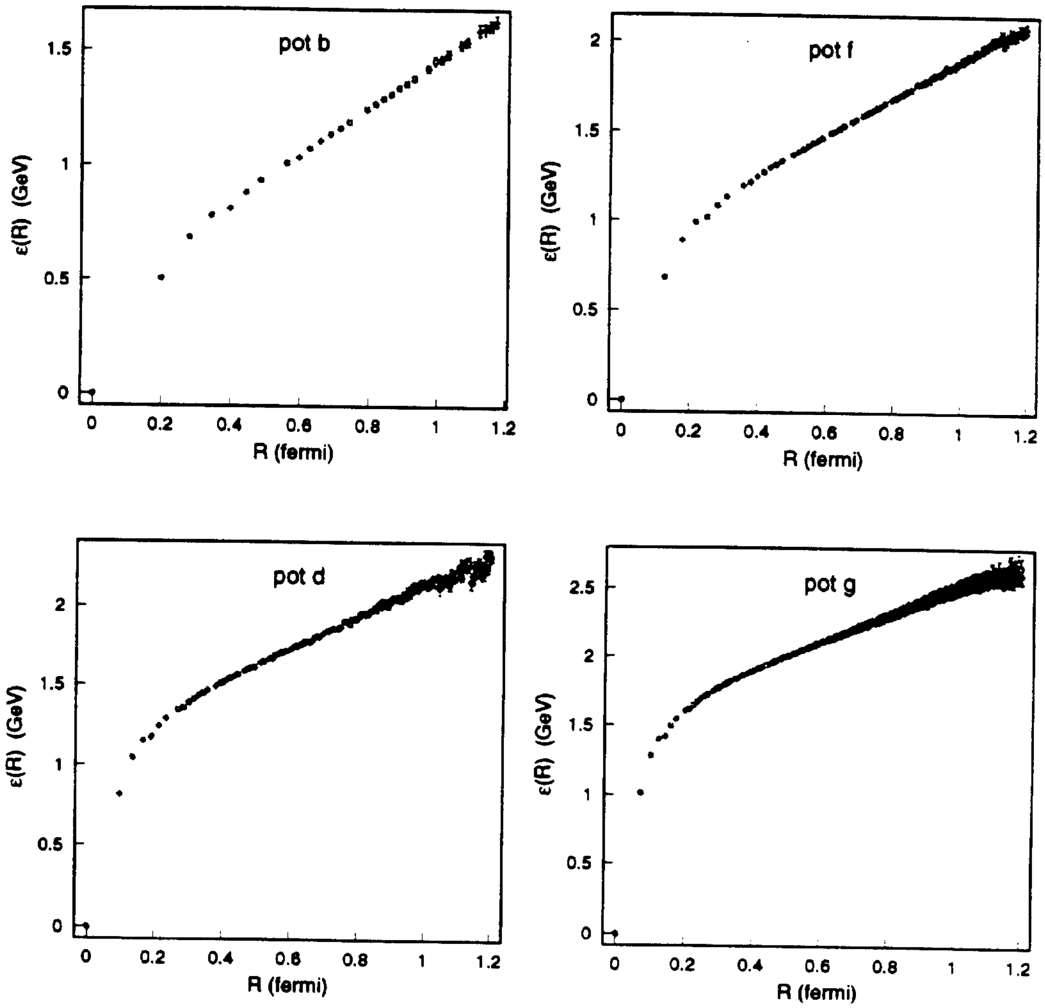

Figure 1: Static potential calculated in Coulomb gauge at $\beta = 5.7, 5.9, 6.1$ and, 6.3 on lattices of size $12^3 \times 24$, $16^3 \times 32$, $24^3 \times 48$, and $32^3 \times 48$, respectively. Errors shown are statistical.

inversion of $E-H$ is performed by the conjugate gradient algorithm, with the multiplication of the kinetic term done in momentum space using a fast Fourier transform.

In most cases we have found it adequate to fit the RQM constituent mass by matching the 1S wavefunction generated by the above procedure to the Coulomb gauge Bethe-Salpeter wavefunction obtained at a roughly fixed Euclidean time (corresponding to time slice 4 at β=5.9). For the particular case of β=5.9, κ=0.159, on a 16^3 lattice, a more detailed fitting procedure was used to determine the optimal choice of quark mass μ in order to fit the meson wavefunction at various time slices. The mean square deviation of $\Psi^{(1S)}_{\rm smear}$ from the measured quenched wavefunctions at various times T, for various μ, is displayed in Table 3.

Table 3: Mean square deviation of RQM smearing and LQCD heavy-light wavefunctions (x10^6), for $\beta = 5.9, \kappa = .159$ as a function of time. μ is the constituent quark mass parameter in the RQM Hamiltonian.

μ	$T=4$	$T=5$	$T=6$	$T=7$	$T=8$
0.05	3.37	1.99	1.36	5.65	5.95
0.10	0.75	0.42	0.20	1.86	2.14
0.12	0.37	0.45	0.36	1.02	1.30
0.15	0.40	1.06	1.15	0.39	0.67
0.20	1.75	3.30	3.61	0.72	1.00

From Table 3 we see that the optimal choice for the constituent quark mass varies in the range 0.10-0.15 if we fit to meson wavefunctions on time slices 4 to 8. We have chosen μ=0.12 as the best compromise for β=5.9, κ=0.159. With this parameter fixed, we have generated, by the procedure outlined following (12), 1S, 2S, 3S and 4S smearing functions to be used in the multistate analysis described in the next section. For other β, κ values, we have usually used two smearing states only. The careful tuning of the quark mass performed here reduces to a very small level (4 percent or less) the coupling of the exact ground state to the higher smearing states, but will not turn out to be essential to the extraction of accurate masses and couplings for the ground state. A detailed discussion of the dependence of the results on the RQM mass parameter chosen for smearing is given in Section 5.1.

As described in a recent article [17], the RQM gives a single-parameter fit to all the excited radial and orbital meson wavefunctions of our heavy-light system. After fixing μ by a match to the 1S wavefunction, we have found remarkable agreement with measured excited state wavefunctions (for example, the 1P state, cf [17]). This agreement suggests that this Ansatz accurately describes at least the valence quark sector of the full mesonic bound-state.

3.2 Multistate Smearing

Our object in this section is to outline a general procedure for extracting the maximum usable information from the multistate correlator matrix:

$$C^{ab}(T) \equiv \sum_{\vec{r}\vec{r}'} \Psi^{(a)}_{\text{smear}}(\vec{r}) < 0 \mid q(\vec{r},T)\bar{Q}(0,T)Q(0,0)\bar{q}(\vec{r}',0) \mid 0 > \Psi^{(b)}_{\text{smear}}(\vec{r}') \qquad (16)$$

where $q(Q)$ are light (heavy) quark operators, and the $\Psi^{(a)}_{\text{smear}}$ (a=1,2,...N) contain the set of orthonormal smearing functions obtained from the RQM as described in the preceding section. From a set of N_c decorrelated gauge configurations, we begin with a corresponding ensemble of N_c statistically independent $C^{ab}(T)$ matrices, from which a standard deviation matrix $\sigma^{ab}(T)$ can be obtained directly. In addition to the smearing wavefunctions of the relativistic potential model, the set $\{\Psi^{(a)}\}$ also includes the local source generating the desired heavy-light axial-vector matrix element for extracting f_B. Other types of smearing (cube, wall, etc) may also be included to facilitate an objective comparison with other recent calculations. In (16), the heavy and light quark propagators in each gauge configuration are computed in Coulomb gauge. As we are dealing with global color singlet states on each time slice (color sums are suppressed) C^{ab} is well-defined and non-zero.

Defining states

$$\mid \Phi^a, T > \equiv \sum_{\vec{r}} \Psi^{(a)}_{\text{smear}}(\vec{r})Q(0,T)\bar{q}(\vec{r},T) \mid 0 > \qquad (17)$$

we have

$$\begin{aligned} C^{ab}(t) &= < \Phi^a, T \mid \Phi^b, 0 > && (18) \\ &= \sum_{n=1}^{M} e^{-E_n T} < \Phi^a \mid n >< n \mid \Phi^b > + O(e^{-E_{M+1}T}) && (19) \end{aligned}$$

where the states $\mid n >$ are exact eigenstates of the lattice Coulomb gauge transfer matrix with eigenvalues e^{-E_n}. The remainder term of order $e^{-E_{M+1}T}$ will of course be small at large Euclidean time, but in addition should have a small prefactor to the extent that our smearing functions $\Psi^{(a)}_{\text{smear}}(\vec{r})$ (a=1,2,..M) do a good job in representing the valence quark structure of the low-lying states, and to the extent that more complicated Fock states (containing extra quark pairs, real gluons, etc) are not too important.

Next, define mixing coefficients (in our case, they are real):

$$v^a{}_n \equiv < \Phi^a \mid n > = < n \mid \Phi^a > \tag{20}$$

Neglecting the exponential contamination of order $e^{-E_{M+1}T}$, we see that the multistate coupling matrix can be fit to an expression of the form

$$C^{ab}(T) = \sum_{n=1}^{M} v^a{}_n v^b{}_n e^{-E_n T} \tag{21}$$

Of course, we cannot hope to extract M independent time-dependencies with $N < M$ smearing wavefunctions, so only $N \geq M$ will be considered. Typically we shall extract the maximum information from the lattice data by picking $N = M + 1$ (the extra source function being the local current needed for the extraction of f_B).

The fit is performed by a chi-square minimization of

$$\chi^2 \equiv \sum_{a,b} \sum_{T=T_<}^{T_>} \frac{\mid C^{ab}(T) - \sum_{n=1}^{M} v^a{}_n v^b{}_n e^{-E_n T} \mid^2}{\sigma^{ab}(T)^2} \tag{22}$$

with respect to the fitting parameters $\{v^a{}_n, E_n\}$, over a fitting range $T_< \leq T \leq T_>$ in Euclidean time. The fit is performed on an ensemble of N_c jack-knife coupling matrices obtained by replacing each in turn of the N_c coupling matrices by the average matrix and reaveraging. We have chosen $\mid \Phi^N > \equiv J_{\rm axial}(0) \mid 0 >$, so the parameters $v^N{}_n$ should be interpreted as *lattice* f-parameters for the ground and excited meson states, E_n as the corresponding masses, and $v^a{}_n$ (a=1,2,..,M) as mixing coefficients indicating the degree of overlap of the exact meson states with our RQM smeared states $\mid \Phi^a >$. The sum over a, b in (22) does *not* include the local-local correlator $a = b = N$, which is not well described by a sum over a few low-lying states. Note that this fitting procedure automatically gives the lattice f-parameters without the need to divide by the square-root of the smeared-smeared correlator as in the usual approach. Moreover, the ensemble of N_c parameter sets $\{v^a{}_n, E_n\}$ obtained in this way can be subjected to a straightforward statistical analysis to determine the error in each of these parameters separately, correlations between parameters (e.g. between masses and f-parameters), and so on.

Once the overlaps $< \Phi^a \mid n >$ have been estimated by a best fit of $C^{ab}(T)$, a smearing operator can be constructed which is guaranteed to contain *at most one* of the first N exact meson states, thereby removing any other exponential time-dependence to the $e^{-E_{N+1}T}$ level. Specifically, if $\epsilon_{a_1 a_2 .. a_N}$ is the totally antisymmetric symbol in N dimensions, the smeared state

$$| \hat{\Phi}^A > \equiv \epsilon_{a_1 a_2 .. a_N} \prod_{i \neq A} v^{a_i}{}_i \, | \, \Phi^{a_A} >, \quad A = 1, 2, ..M \tag{23}$$

is guaranteed (to the extent that we have accurately extracted the mixing coefficients $v^a{}_n$) to contain only the exact meson state $| \, A >$, together with contaminations from the $(N+1)$'th excited state and higher. An effective mass plot of the usual kind can then be obtained for the A'th state by displaying (we use a smeared-local correlator to minimize noise)

$$m^A_{\text{eff}}(T) \equiv \ln \frac{C^A(T-1)}{C^A(T)} \tag{24}$$

where

$$C^A(T) = < \hat{\Phi}^A, T \, | \, \Psi^{(\text{loc})}, 0 > \tag{25}$$

Of course, this plot will be most flat for the ground state $A = 1$, where the relative exponential contamination is reduced to the level $e^{-(E_{N+1}-E_1)T}$, and where small admixtures of lower-lying states cannot creep in to distort the effective mass plateau. The effective mass plots for the ground state at $\beta = 5.7, 5.9, 6.1$, and 6.3 for various kappa values are shown in Figs.[2-7]. The solid line in each of these plots represents the ground state energy extracted from the full multistate fit over the time window indicated by the length of the line. For each β the time window for the multistate fit was chosen to be over approximately the same interval in physical units, viz. about $\frac{1}{3} fm$ to $1 fm$. Noting that the splitting between the ground state and the second excited state is found, in our multistate calculations, to be around 800 to $900 MeV$, the choice of $\frac{1}{3} fm$ for the lower end of the time window should provide an exponential supression of excited states by at least a factor of 3. In addition, our careful tuning of the smearing functions should produce a relatively small coefficient for the higher excited states. The equality of the smeared-smeared and smeared-local effective masses exhibited in the plots confirms our choice of fitting interval. A more complete discussion of systematic errors due to excited states is given in Section 5.1.

The fitting formula (22) is easily generalized to allow a global fit to the data at various κ values (for fixed β): this is essential in order to take into account correlations between the coupling matrices at different κ values, which would affect our estimate for the error of the

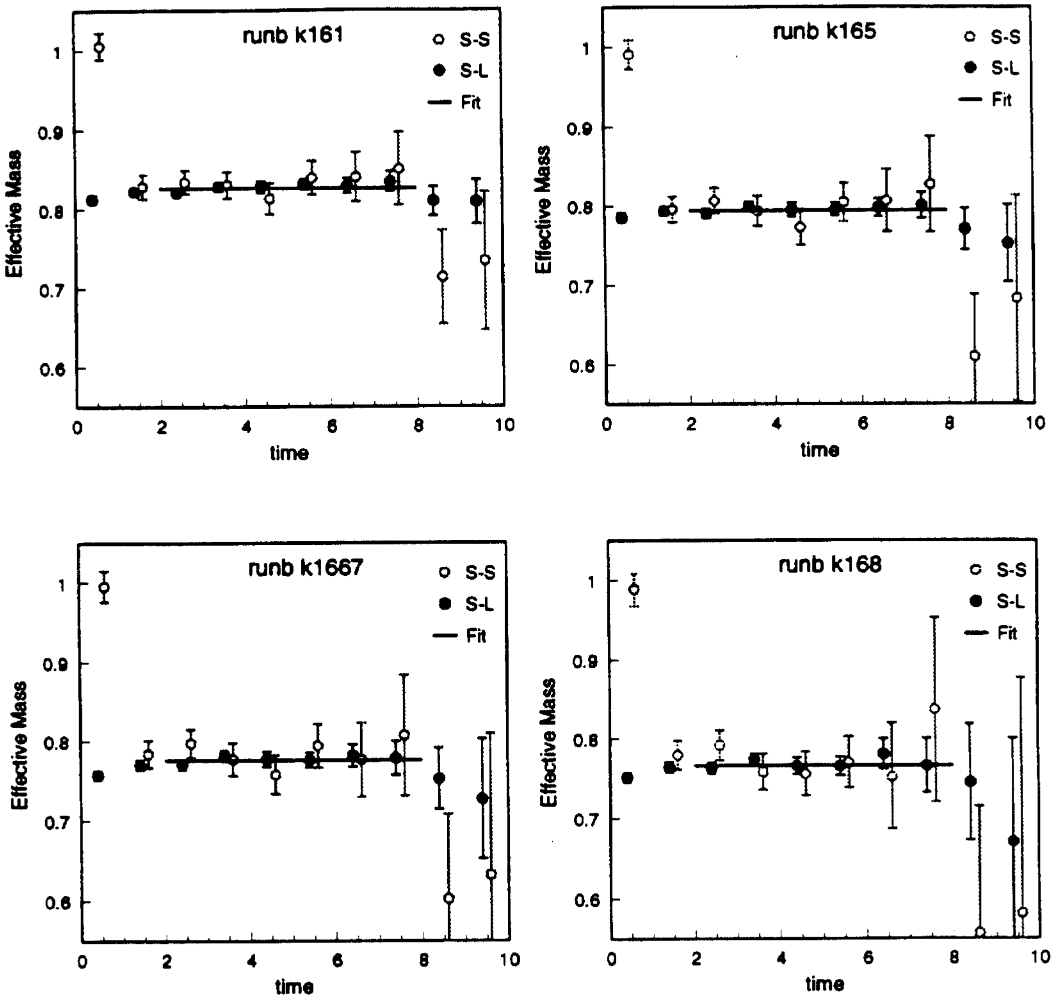

Figure 2: Smeared-smeared (S-S) and smeared local (S-L) effective masses for $\beta = 5.7, 12^3 \times 24$, and $\kappa = .161, .165, .1667$, and $.168$. Solid line is the ground state energy extracted from a 2-state fit. Smearing functions are optimized combinations of RQM wavefunctions, as described in the text.

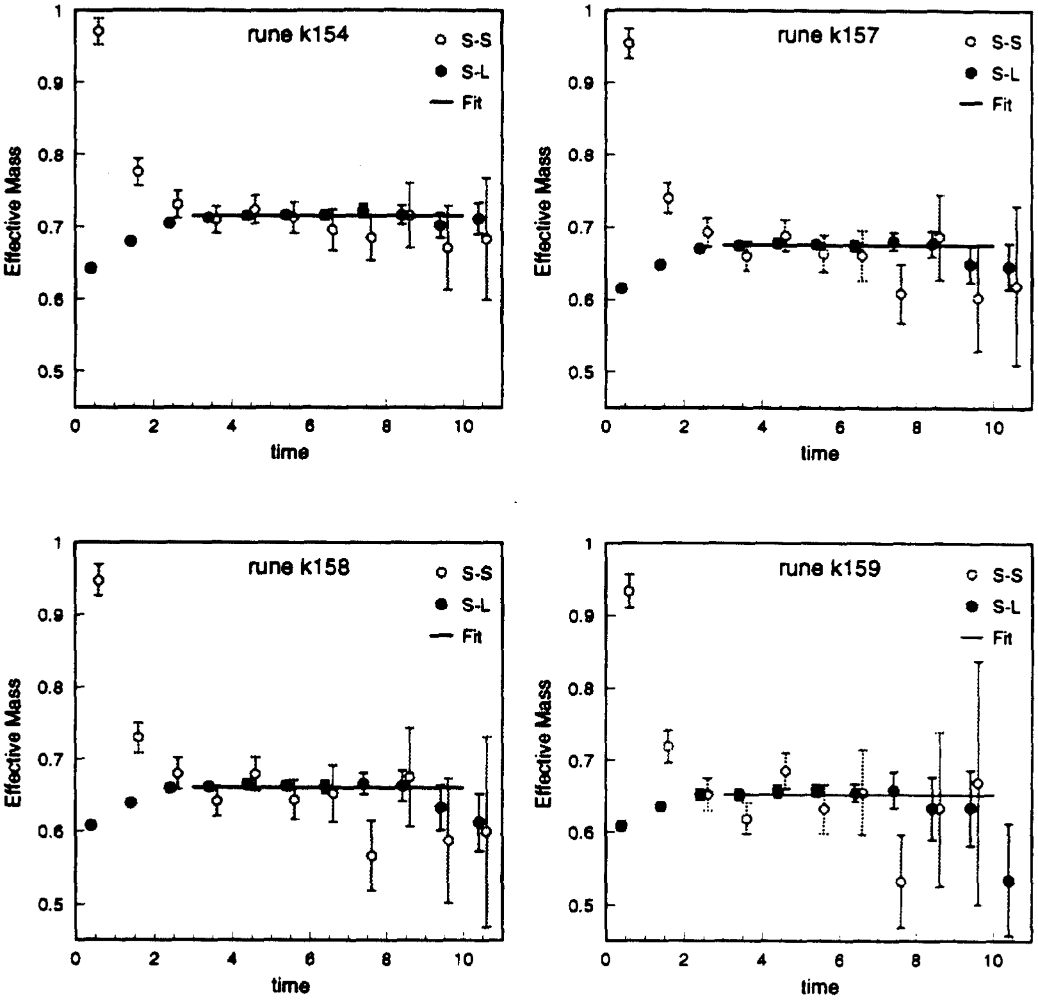

Figure 3: Smeared-smeared (S-S) and smeared local (S-L) effective masses for $\beta = 5.9, 12^3 \times 24$, and $\kappa = .154, .157, .158$, and $.159$. Solid line is the ground state energy extracted from a 2-state fit. Smearing functions are optimized combinations of RQM wavefunctions, as described in the text.

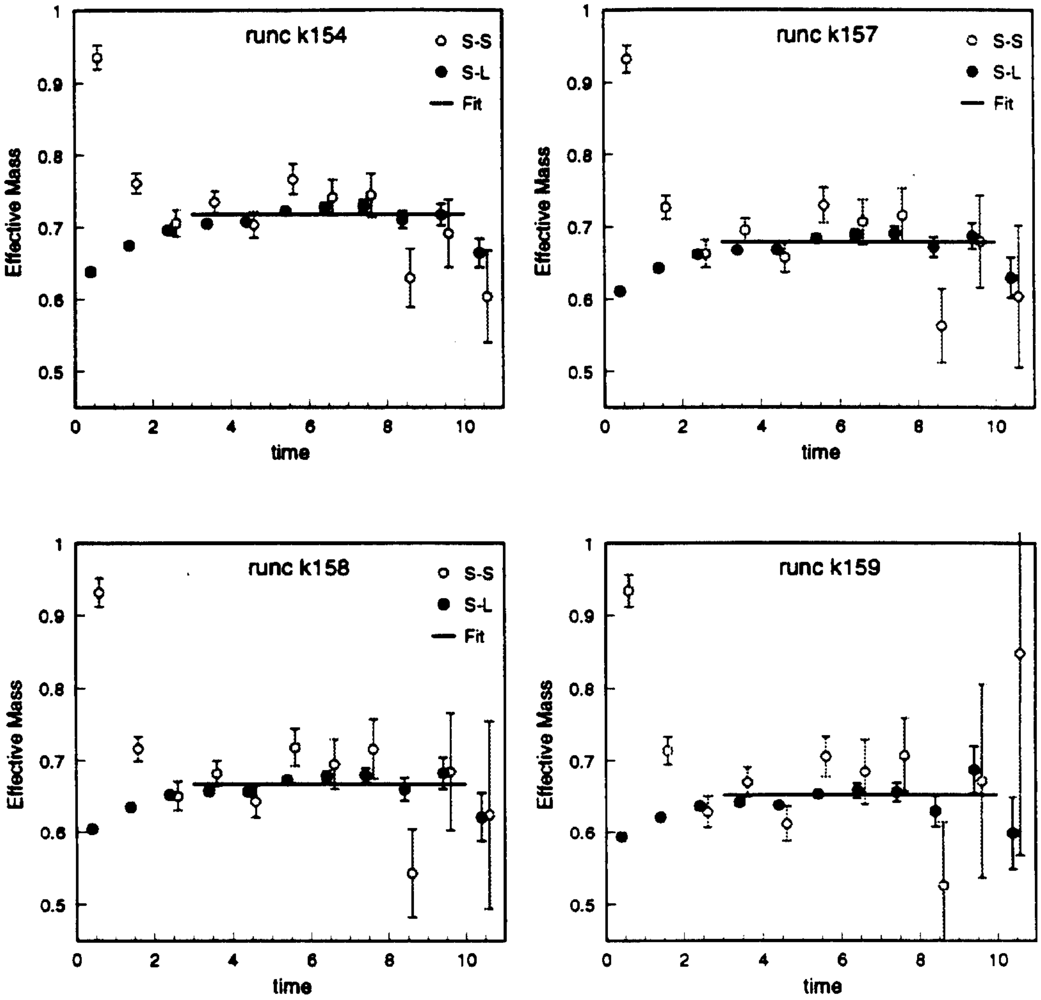

Figure 4: Smeared-smeared (S-S) and smeared local (S-L) effective masses for $\beta = 5.9, 16^3 \times 32$, and $\kappa = .154, .157, .158$, and .159. Solid line is the ground state energy extracted from a 2-state fit. Smearing functions are optimized combinations of RQM wavefunctions, as described in the text.

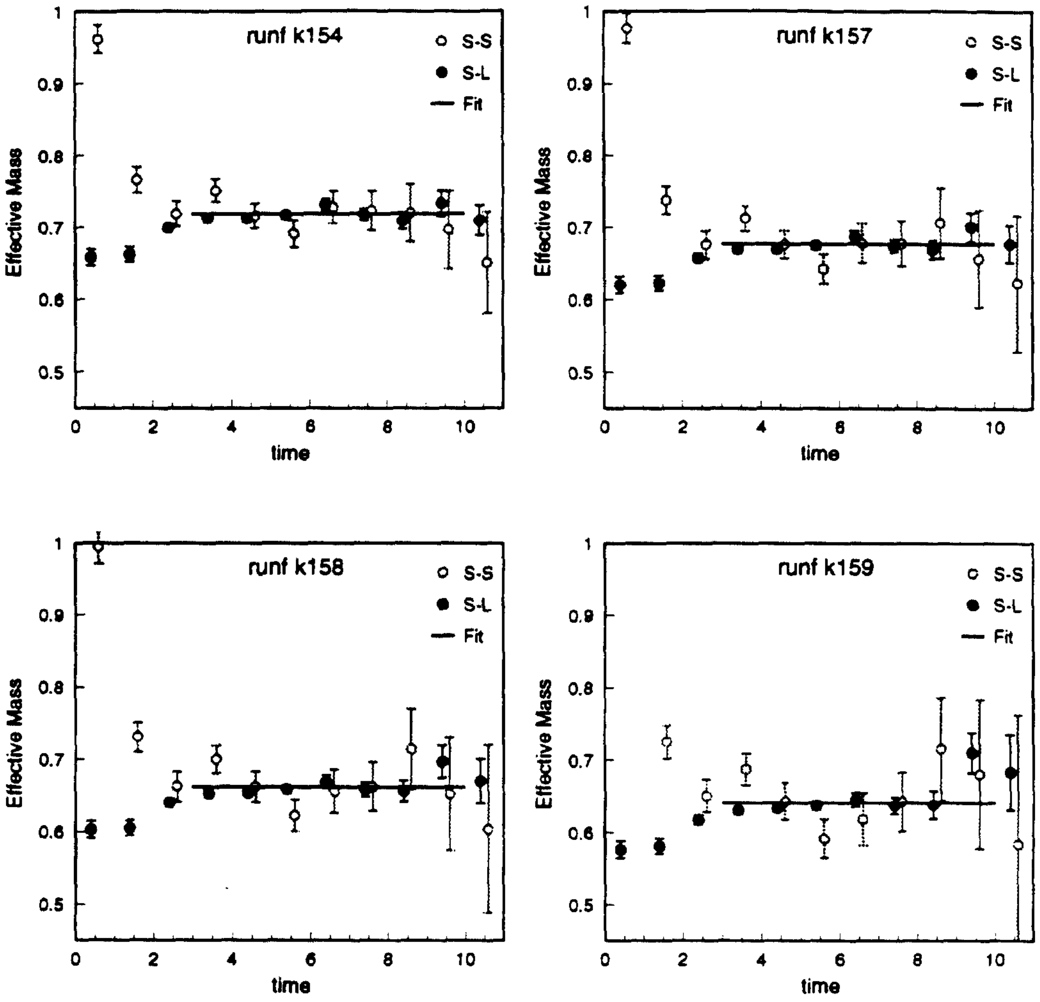

Figure 5: Smeared-smeared (S-S) and smeared local (S-L) effective masses for $\beta = 5.9, 20^3 \times 40$, and $\kappa = .154, .157, .158$, and $.159$. Solid line is the ground state energy extracted from a 2-state fit. Smearing functions are optimized combinations of RQM wavefunctions, as described in the text.

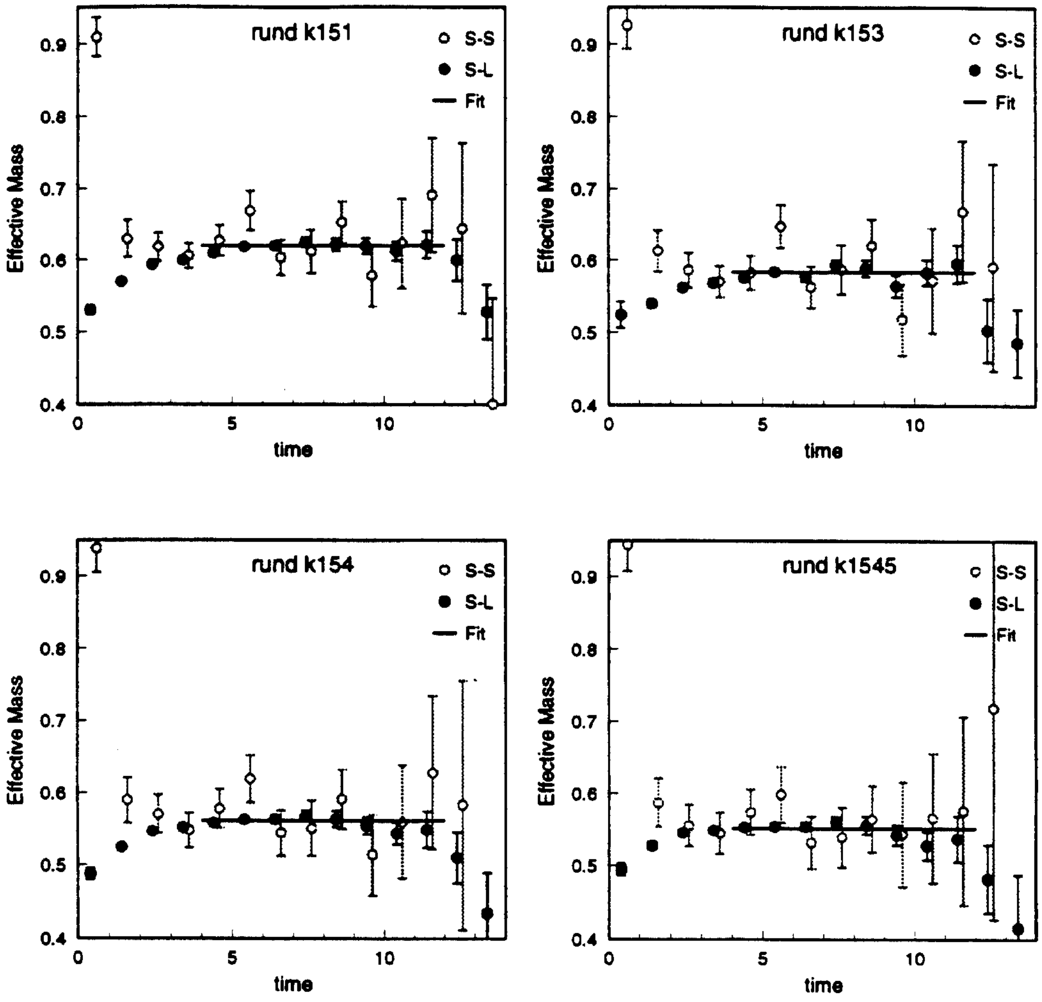

Figure 6: Smeared-smeared (S-S) and smeared local (S-L) effective masses for $\beta = 6.1, 24^3 \times 48$, and $\kappa = .151, .153, .154$, and .1545. Solid line is the ground state energy extracted from a 2-state fit. Smearing functions are optimized combinations of RQM wavefunctions, as described in the text.

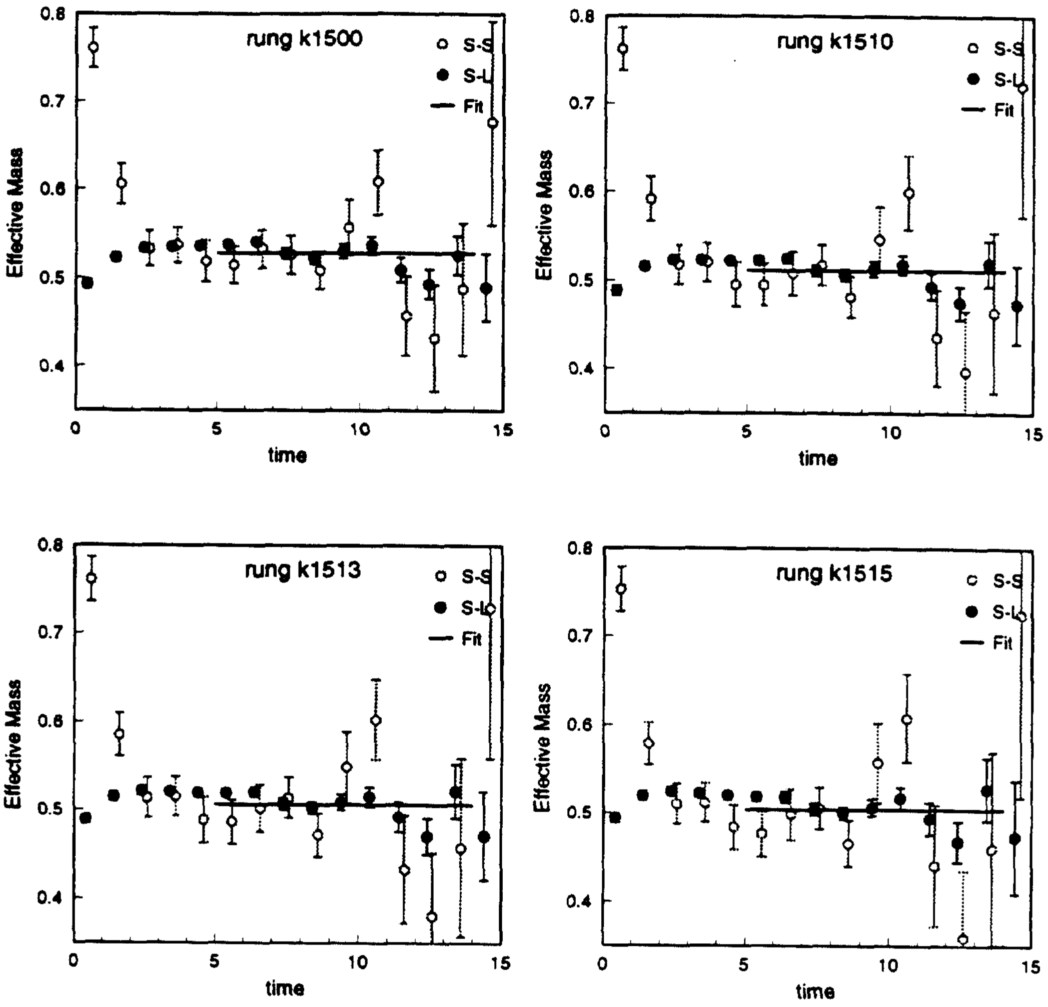

Figure 7: Smeared-smeared (S-S) and smeared local (S-L) effective masses for $\beta = 6.3, 32^3 \times 48$, and $\kappa = .1500, .1500.1513$, and .1515. Solid line is the ground state energy extracted from a 2-state fit. Smearing functions are optimized combinations of RQM wavefunctions, as described in the text.

results when linearly extrapolated to κ_c. Namely, (22) is replaced by

$$\chi^2 \equiv \sum_{a,b} \sum_{\kappa} \sum_{T=T_<}^{T_>} \frac{\mid C^{ab}(\kappa,T) - \sum_{n=1}^{M} v^a{}_n(\kappa) v^b{}_n(\kappa) e^{-E_n(\kappa)T} \mid^2}{\sigma^{ab}(\kappa,T)^2} \tag{26}$$

where

$$\begin{aligned} v^{a=N}_{n}(\kappa) &\equiv v^a_0{}_n + v^a_1{}_n(\kappa^{-1} - \kappa_c^{-1}) \\ E_n(\kappa) &\equiv E_0{}_n + E_1{}_n(\kappa^{-1} - \kappa_c^{-1}) \end{aligned}$$

and the mixing coefficients $v^{a=1,..M}_{n}$ are varied freely. Note that only the immediately physical mass and lattice-f parameters are assumed to have the chiral dependence on κ^{-1}: other mixing coefficients involve the model dependent choice of smearing functions from the RQM. The chi-square minimization allows the direct extraction of masses and couplings extrapolated to κ_c, as well as the slopes in κ^{-1} of these quantities (all of which are free variational parameters in this new global fitting procedure). The usual jackknife procedure can then be applied to yield the correct errors on the extrapolated quantities.

4 Lattice Results for Heavy-Light Mesons

To extract results for masses and decay constants we have used the set of gauge configurations and light quark propagators enumerated in Table 4. The light quark action we use is not $O(a)$ improved. The four columns in Table 4 are the gauge coupling, β; lattice size; number of gauge configurations (separated by 1000, 2000, 4000, and 4000 sweeps for $\beta = 5.7$, 5.9, 6.1, and 6.3 respectively); and the light quark κ values calculated for each configuration.

Table 4: Summary of gauge configurations and light quark parameters used in this paper. Listed are a letter used to identify each Monte Carlo run, the β value, lattice size, number of gauge configurations in each ensemble, and the values of light quark hopping parameter κ analyzed.

run	β	lattice	confs	κ
b	5.7	$12^3 \times 24$	100	.168,.1667,.165,.161
e	5.9	$12^3 \times 24$	100	.159,.158,.157,.154
c	5.9	$16^3 \times 32$	100	.159,.158,.157,.156,.154
f	5.9	$20^3 \times 40$	100	.159,.158,.157,.154
d	6.1	$24^3 \times 48$	50	.1545,.154,.153,.151
g	6.3	$32^3 \times 48$	50	.1515,.1513,.1510,.1500

The multistate smearing analysis outlined in Section 3 provides a powerful method for extracting heavy-light meson parameters. Unlike single or double exponential fits to single-channel "smeared-smeared" and "smeared-local" correlators, the fitting of the $N \times N$ matrix of correlators to an expression of the form (21) is highly constrained. As we will show, this method allows a determination of f_B and other heavy-light parameters which is less prone to systematic errors than previously applied methods. In this section, we present our results. In Section 6.2 we compare these results with those recently reported in Refs.[12, 14, 19, 41]. Most of the results presented here were obtained from the fitting procedure discussed in Section 4 using $N = 3$ and $M = 2$, i.e. a 3×3 matrix of correlators (2 smearing functions and the δ-function source) fit to the sum of two exponentials (always excluding the local-local correlator from the fit). To estimate the systematic errors associated with the fitting procedure, we have tried varying both the shape of the smearing functions (by adjusting the RQM quark mass parameter) and the number M of smearing functions included. These results are discussed below.

First consider the mass eigenvalue E_1 in Eq. (22) which describes the leading exponential falloff of the heavy-light correlators

$$C^{ab}(t) \simeq v_1^a v_1^b e^{-E_1 t} \tag{27}$$

In the multistate fitting procedure, E_1 is the energy associated with the ground state contribution to the correlator. This parameter represents a combination of the binding energy of the B-meson ground state plus a divergent mass shift of the heavy quark. Recall that only the bare mass of the heavy quark is removed in reducing to the effective static theory. The mass shift induced by QCD is therefore measureable on the lattice as a non-scaling piece in the parameter E_1. We measure the dependence of E_1 on both the light-quark hopping parameter κ and the lattice spacing a. The graph in Fig. 8 shows the κ-dependence of E_1 for the four values of β studied. In each of the four data sets, the dependence on κ^{-1} is quite linear, allowing an accurate extrapolation to the chiral limit κ_c. Numerical results are tabulated in Table 5. For each value of beta and kappa the results in this table were obtained from a 2-state fit, with the χ^2 per degree of freedom of each fit listed in the last column. For $\beta = 5.9$, the χ^2/dof are those obtained on the 20^3 box. The results for $\tilde{f}_B$ and aE_1 at $\beta = 5.9$ listed in Table 5 are the infinite volume values obtained by fitting all three box sizes to a Luscher finite volume formula, as described in Section 5.2 (except for $\kappa = .156$, which has only been done on the 16^3 box). The results for the three box sizes are listed separately in Tables 7 and 8. A measure of the overlap between the true ground state and the RQM wavefunction smeared operators is given by $\sqrt{2\kappa}\left[\sum_{a=1}^{M}(v_1^a)^2\right]^{\frac{1}{2}}/\sqrt{6}$. The measured values of this overlap for each of the fits is recorded in Table 5.

In addition to analyzing the data at each value of κ separately, we have also performed a simultaneous fit to all κ values for a given β by allowing the multistate fitting parameters v_n^a to depend on κ, as described in Section 3. Using this procedure on jackknifed subensembles provides a better estimate of the error on the chiral extrapolation, since it takes account of the fact that the different κ values have correlated errors. Comparing the results of this analysis with results of a separate analysis of each κ, we find that the extrapolated values for E_1 and f_B change very little, while the error bars on these results are about 30% lower than those obtained by ignoring κ correlations. On the other hand, the results for the

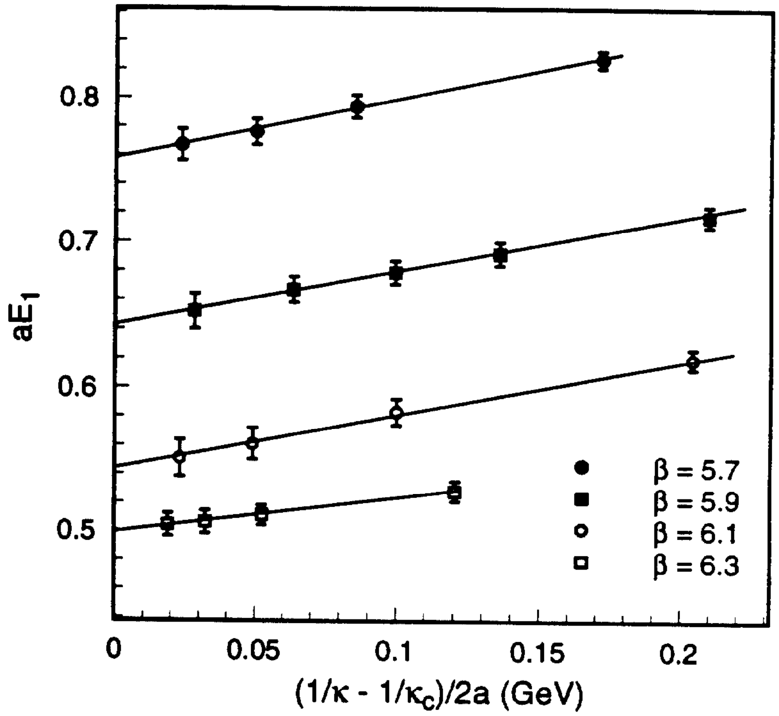

Figure 8: Heavy-light ground-state energy aE_1 vs. bare quark mass for $\beta = 5.7, 5.9, 6.1$, and 6.3 Each data point is the ground state energy extracted from a two-state fit. Error bars are statistical only. Solid lines are obtained from a simultaneous two-state fit to all kappa values for a given β as described in the text.

Table 5: Lattice results for heavy-light mesons (static approximation). Values for the ground state energy aE_1 and decay constant $\tilde{f}_B$ are extracted from a 2-state fit over time window ΔT. ($\tilde{f}_B$ is related to the physical decay constant f_B by Eq. (30)). Results at $\kappa = \kappa_c$ are from the multi-κ fits as discussed in Sec. 3.2. The column labeled *overlap* is a measure of the total overlap between the true ground state and the RQM wavefunction smeared operators used.

β	ΔT	κ	aE_1	*overlap*	$\tilde{f}_B$	χ^2/dof
5.7	2-8	.161	.827(6)	.725(7)	.670(19)	.50
		.165	.794(8)	.717(8)	.626(23)	.78
		.1667	.776(9)	.699(7)	.590(24)	.54
		.168	.767(11)	.694(9)	.578(29)	.43
		κ_c	.758(10)	.694(8)	.564(28)	.58
5.9	3-10	.154	.719(5)	.742(12)	.347(11)	.87
		.156	.692(8)	.731(13)	.318(13)	1.06
		.157	.678(6)	.724(13)	.300(11)	.62
		.158	.665(7)	.716(15)	.283(12)	.56
		.159	.645(9)	.704(18)	.259(14)	.60
		κ_c	.638(9)	.686(24)	.250(14)	.66
6.1	4-12	.151	.620(7)	.769(17)	.199(10)	.57
		.153	.583(9)	.721(24)	.170(12)	.60
		.154	.561(11)	.705(24)	.149(12)	.61
		.1545	.551(13)	.700(30)	.142(14)	.48
		κ_c	.544(12)	.689(25)	.135(13)	.55
6.3	5-14	.1500	.528(7)	.748(18)	.120(7)	.72
		.1510	.511(7)	.728(20)	.107(7)	.66
		.1513	.506(8)	.724(20)	.104(7)	.61
		.1515	.504(8)	.729(20)	.103(8)	.56
		κ_c	.499(9)	.720(17)	.099(8)	.62

slope of these quantities as a function of κ^{-1} are greatly improved by the simultaneous-κ fit, reducing the errors by a factor of 3 or more over the independent-κ analysis. Thus it is especially important to take account of inter-κ correlations for quantities such as $m_{B_s} - m_{B_u}$ and f_{B_s}/f_{B_u}.

Let us consider E_1 as a function of the lattice spacing a and of the naive light quark mass (see Appendix). The linear dependence on κ^{-1} becomes

$$\begin{aligned} E_1(2am_q, a) &= E_1(0,a) + (\kappa^{-1} - \kappa_c^{-1})E_1'(0,a) \\ &= E_1(0,a) + 2am_q E_1'(0,a) \end{aligned} \tag{28}$$

The quantity M_{eff} defined in Section 2, Eq. (6) is just E_1 evaluated at $\kappa = \kappa_c$,

$$M_{eff} = E_1(0,a) \tag{29}$$

The slope parameters $E_1'(0,a)$ are obtained by a correlated fit to all κ-values, as described in Section 3. The results for the slopes and intercepts are given in Table 6.

Table 6: Slopes and intercepts for aE_1 and $\tilde{f}_B$ as a function of $\kappa^{-1} - \kappa_c^{-1}$. For a given β,values are obtained from a simultaneous two-state fit to all values of κ over a time window ΔT.

β	ΔT	$aE_1(0)$	$E_1'(0)$	$\tilde{f}_B(0)$	$\tilde{f}_B'(0)$
5.7	2-8	.758(11)	.236(25)	.564(29)	.424(72)
5.9	3-10	.638(9)	.350(25)	.250(13)	.444(38)
6.1	4-12	.544(12)	.450(47)	.138(13)	.387(46)
6.3	5-14	.499(9)	.376(56)	.099(7)	.290(56)

In a similar way, we obtain a linear fit (see Fig. 9) to the κ^{-1} dependence of the groundstate pseudoscalar decay constant f_B. Define a quantity $\tilde{f}_B$ which is just the matrix element parameter v_1^N in the multistate fit (overlap of the ground state with the δ-function source), with a normalization factor $\sqrt{2\kappa}$ for the light quark included. In the scaling limit, the physical value of f_B is related to $\tilde{f}_B$ by the following multiplicative constants,

$$f_B = \tilde{f}_B \times \sqrt{\frac{2}{M_B}} \times a^{-\frac{3}{2}} \times Z_A \tag{30}$$

where Z_A is the renormalization factor associated with matching the full theory with the effective static theory on the lattice, as discussed in [34], [42], and in Section 2.

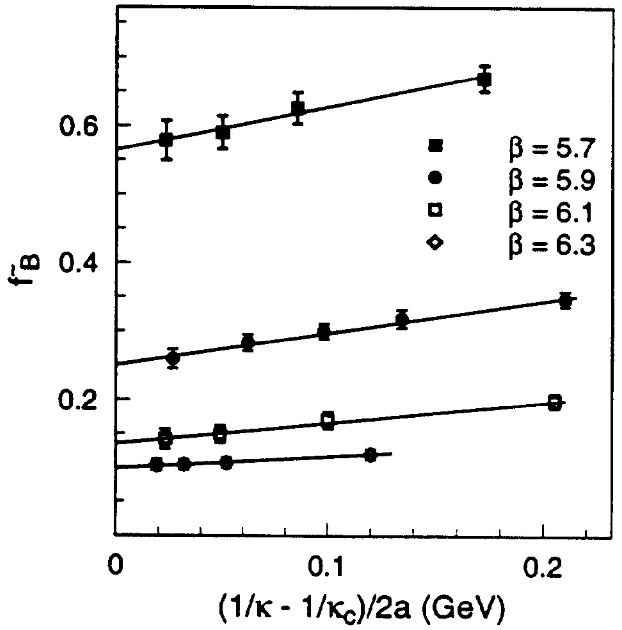

Figure 9: $\tilde{f}_B$ as a function of bare quark mass for the four runs $\beta = 5.7, 5.9, 6.1$, and 6.3. Data points are decay constants extracted from a two-state fit. Error bars are statistical only. Solid lines are obtained from a simultaneous fit to all kappa values for a given beta as described in the text.

The lattice spacing dependence of E_1 in the chiral limit $m_q = 0$ is plotted in Fig. 10. The results are consistent with a linear a dependence,

$$aE_1(0,a) = E_1(0,0) + \tilde{E}_1 a \tag{31}$$

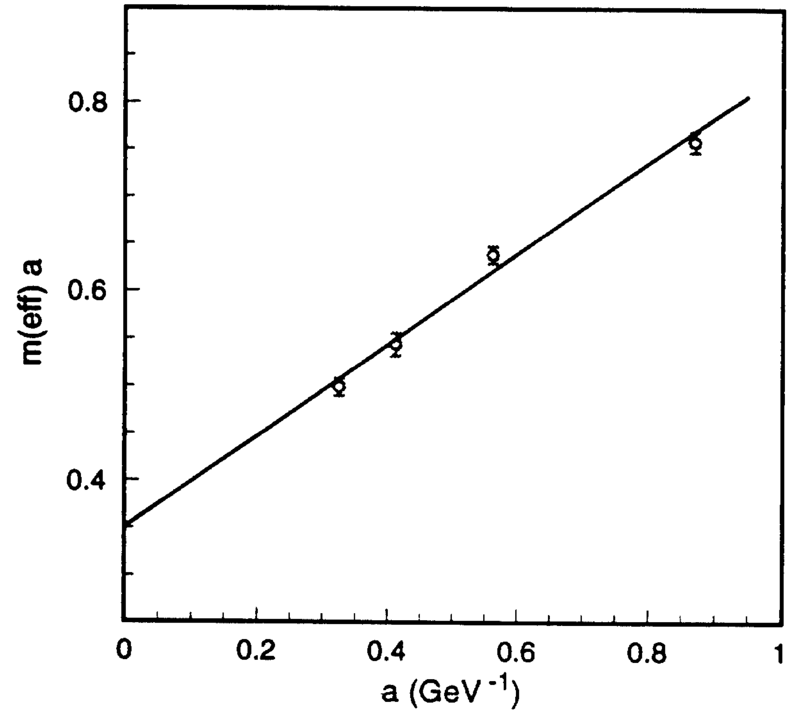

Figure 10: Heavy-light ground-state energy at $\kappa = \kappa_c$ vs. lattice spacing for $\beta = 5.7, 5.9, .6.1$, and6.3. Solid line represents a minumum-χ^2 linear fit to the four data points.

with

$$E_1(0,0) = .351(14) \tag{32}$$

$$\tilde{E}_1 = .481(25)\text{GeV} \tag{33}$$

The first term $E_1(0,0)$ is the linearly divergent (i.e. $O(1/a)$) term in the heavy quark mass shift.

The tadpole-improved estimate of $a\delta m$ was discussed in Section 2. The corresponding quantity is $a\widetilde{\delta m} + \ln u_0$, and was tabulated in Table 2. Comparing the ground state effective mass with the tadpole improved 1-loop result at each lattice spacing one finds about a 30 % discrepancy in the singular part of the mass shift, which can easily be accounted for by higher-loop and/or nonperturbative contributions. In fact, ordinary (non-improved) one-loop perturbation theory [34] gives

$$\delta m = -\frac{1}{a} \times \frac{g^2}{12\pi^2} \times 19.95 \tag{34}$$

Simply identifying this value with the extrapolated lattice result gives $\alpha_s \simeq 0.162(6)$ which is in reasonable agreement with other determinations of α_s in the range of lattice spacings considered here [20]. So the entire "discrepancy" can be removed by a reasonable redefinition of the perturbative coupling being used.

The mass of the meson B_s, composed of a b quark and a strange antiquark, is of considerable phenomenological interest. Our calculation of the heavy-light ground state energy as a function of κ provides a determination of the mass splitting between the B_s and the B_u mesons

$$\Delta M_{B_s} = M_{B_s} - M_{B_u} \tag{35}$$

Since the divergent self-mass of the heavy quark is independent of light quark mass, it will cancel in the mass difference ΔM_{B_s}, and the latter should therefore scale properly with a. For each value of β, we use the determination of κ_s and κ_u discussed in the Appendix, along with the observed κ dependence of E_1 to determine ΔM_{B_s}. The results are shown in Fig. 11.

A linear extrapolation of the mass difference ΔM_{B_s} to $a = 0$ gives

$$\Delta M_{B_s} = 86 \pm 12 \text{ MeV} \tag{36}$$

Notice that the results for ΔM_{B_s} shown in Fig. 11 exhibit a fairly mild dependence on the lattice spacing, in marked contrast to the strong a-dependence of f_B. The decay constant f_{B_s} for the strange B-meson may be determined, using the values for the slope parameter $\tilde{f}'_B$ in Table 6. The ratio f_{B_s}/f_{B_u} is plotted in Fig. 12. Again, the a-dependence of the ratio is much weaker than that of f_B itself. Extrapolating to $a = 0$, we obtain

$$\frac{f_{B_s}}{f_{B_u}} = 1.216 \pm 0.041 \tag{37}$$

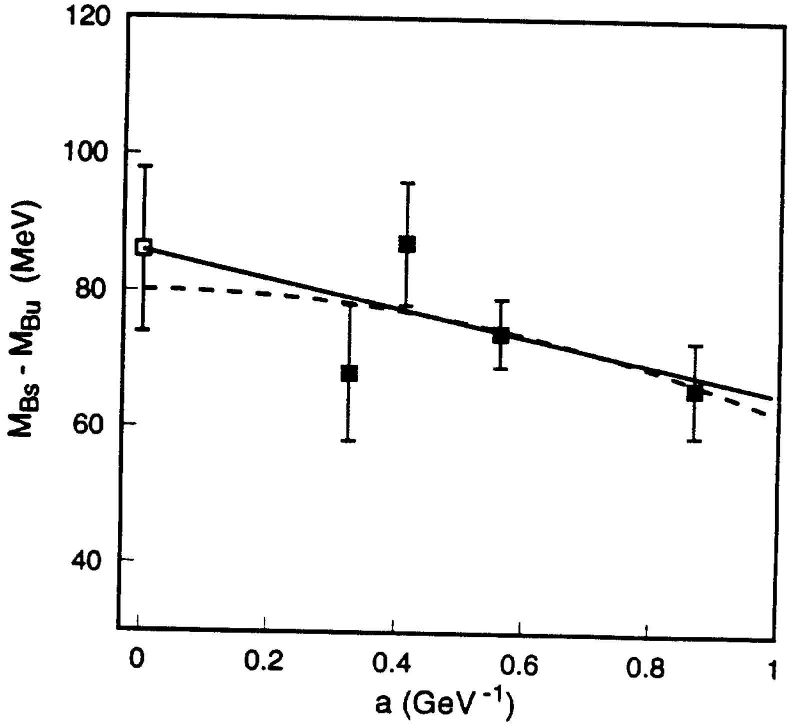

Figure 11: $M_{B_s} - M_{B_u}$ vs. lattice spacing. Solid line is the best linear fit. Dashed line is a quadratic fit (a^2) used to estimate systematic error in $a \rightarrow 0$ extrapolation (See Section 5.5).

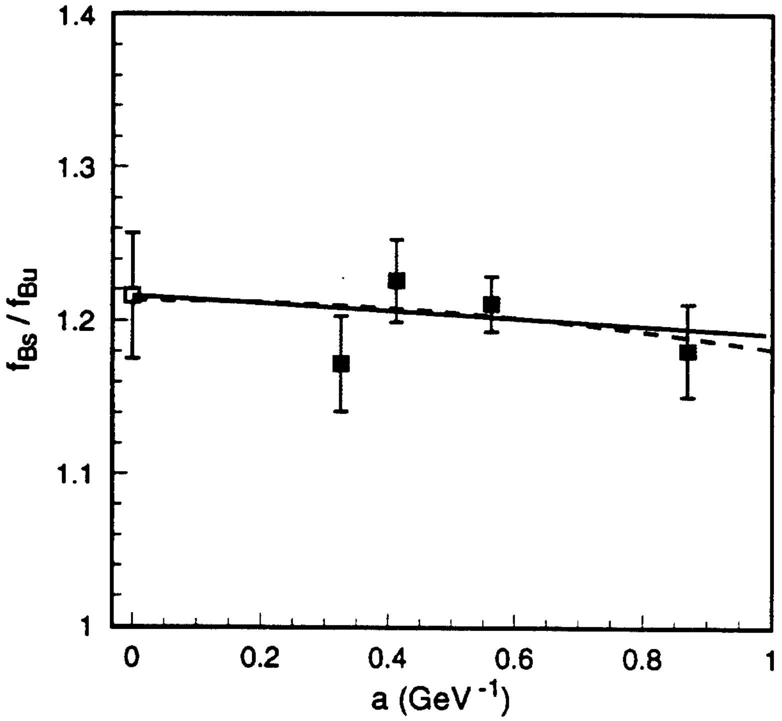

Figure 12: f_{Bs}/f_{Bu} vs. lattice spacing. Solid line represents the best linear (a) fit. Dashed line is a quadratic fit (a^2) used to estimate systematic error in $a \to 0$ extrapolation (See Section 5.5).

5 Determination of Systematic Errors

5.1 Systematic error due to excited state contamination

The main results presented for f_B have been obtained by a 2-state fit to the correlators which employed quark-model smearing functions for the ground state (1S) and first radially excited (2S) state. As pointed out in Section 3, this produced quite stable effective mass plots which indicated that accurate ground state parameters could be extracted with time separations as short as $T = 2$ or 3. Since the errors in most previous calculations have been dominated by the systematic effect of higher state contamination, it is particularly important to estimate the size of this effect to get an overall determination of the accuracy of our results. To further investigate this issue, we have carried out a more complete study of the dependence of the extracted $\tilde{f}_B$ value on the fitting procedure. First, we have varied the size of the source smearing function by changing the quark mass parameter μ in the RQM wavefunctions. We then compare the results from the 2-state fit with those from a truncated 1-state fit (using only the correlators of the ground state smearing function and the delta-function source).

In Figure 13 we compare the effective mass from the 1-state fit with that of the 2-state fit. After determining the 1S-2S splitting Δ from a 2-state fit, the effective masses obtained over a Euclidean time window can be plotted versus the variable $e^{-\Delta t}$, allowing an extrapolation to $t = \infty$ (See below). The results of the 1-state fit are plotted for four different time windows, 1-6, 2-7, 3-8, and 4-9, and for four different choices of RQM smearing functions (with quark mass $\mu = .32, .60, .90$, and 1.20). (Note: The result from window $t_< - t_>$ is plotted at the value of $e^{-\Delta t}$ corresponding to $t = t_<$.) The effective masses from the 2-state fit using the four different μ values and the time window 3-10 are all plotted on the far left side of the plot at $e^{-\Delta t} = 0$. The 1-state results for the different smearing function choices are clearly converging to a common effective mass at $t = \infty$ which agrees well with the 2-state result, the latter being quite insensitive to the choice of μ. Similarly, the result for f_B from the full 2-state fit remains unchanged, within errors, for a wide variation of the μ parameter. On the other hand, the result from the 1-state fit varies by 20-30 % over the same range of μ values. This provides strong evidence that the 2-state fit does a good job of isolating the ground state, even when the chosen smearing functions are not very well tuned. To demonstrate this, we look at the dependence of these results on the time window chosen

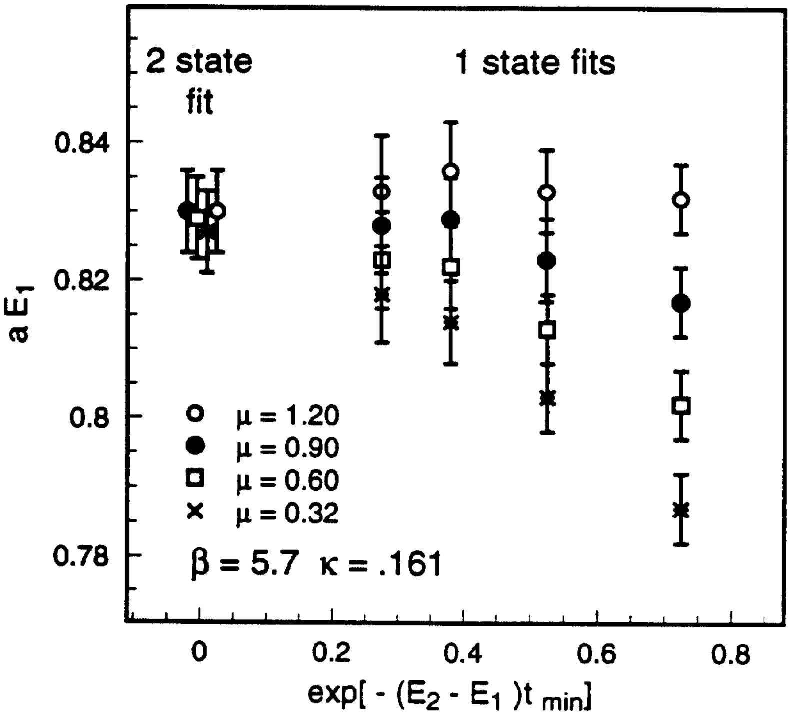

Figure 13: Time-window dependence of effective mass for 1-state fits compared with 2-state fits for $\beta = 5.7, \kappa = .161$. The four sets of points represent the different values of RQM mass parameter μ used to construct smearing functions. One-state fits were obtained from time-windows (reading from right to left on the graph) 1-6, 2-7, 3-8, 4-9. Points are plotted at $\exp[-(\Delta E)t_{min}]$, where $\Delta E = E_2 - E_1$ is the splitting of the first excited (2S) state from the ground-state and t_{min} is the smallest time included in the fit. The 2-state fits were obtained from the window 2-8 but are plotted here at $t \approx \infty$ to illustrate the convergence of the 1-state effective mass to the essentially μ independent 2-state value.

for fitting. While the two-state fits are generally stable under variation of the time window, the 1-state fit shows a systematic time-dependence. If this time-dependence is assumed to be largely due to contamination from the first excited state, it should fit asymptotically to the functional form

$$\tilde{f}_B(t) = \tilde{f}_B(\infty) + Ce^{-\Delta t} \tag{38}$$

where $\Delta = E_2 - E_1$ is the energy splitting between the ground state and first excited state. Without an independent estimate of this splitting, it is difficult to obtain a reliable determination of the parameters in (38) directly from the results of the 1-state fit. On the other hand, the 2-state fit determines both E_1 and E_2, and therefore Δ. If we use this determination to fix Δ, the formula (38) can be used to extrapolate the 1-state results to $t = \infty$. Comparing this result with that of the full 2-state fit provides a useful and nontrivial check on the assertion that the systematic effect from excited states is under control. Figure 14 shows the results of such a comparison for the case $\beta = 5.7, \kappa = .161$. The splitting obtained from the 2-state fit is $\Delta = .321$ in lattice units. It is seen in Fig. 14 that, for the time window 1-6 (far right on the graph), the result for $\tilde{f}_B$ varies systematically with the choice of smearing function. As t gets larger, the results from the different smearing functions tend to converge to the same value. The points plotted at $e^{-\Delta t} = 0$ include the four extrapolated values obtained from Eq. (38). For comparison, the results of the 2-state fit for the four μ values and $t = 3 - 10$ are also plotted. All of these points are well within a standard deviation of each other. Similar comparison of the results of 1-state and 2-state fits for other values of β and κ give comparable agreement. Based on this agreement, we conclude that the systematic error on our results due to excited states has been eliminated at the level of our present statistics.

It is worth emphasizing here that our ability to control excited state contamination depends crucially on the use of the multi-state fitting procedure. Although the 1-state fits were all found to lead to consistent results after extrapolation to $t = \infty$, an accurate extrapolation would not have been possible without an independent determination of the splitting Δ, which is only obtainable from the 2-state fit.

5.2 Finite volume corrections

Using the scales in Table 1, we find that the physical volumes of the boxes for the main ensembles used in our calculation are approximately $(2.0fm)^3$, $(1.8fm)^3$, $(1.9fm)^3$, and

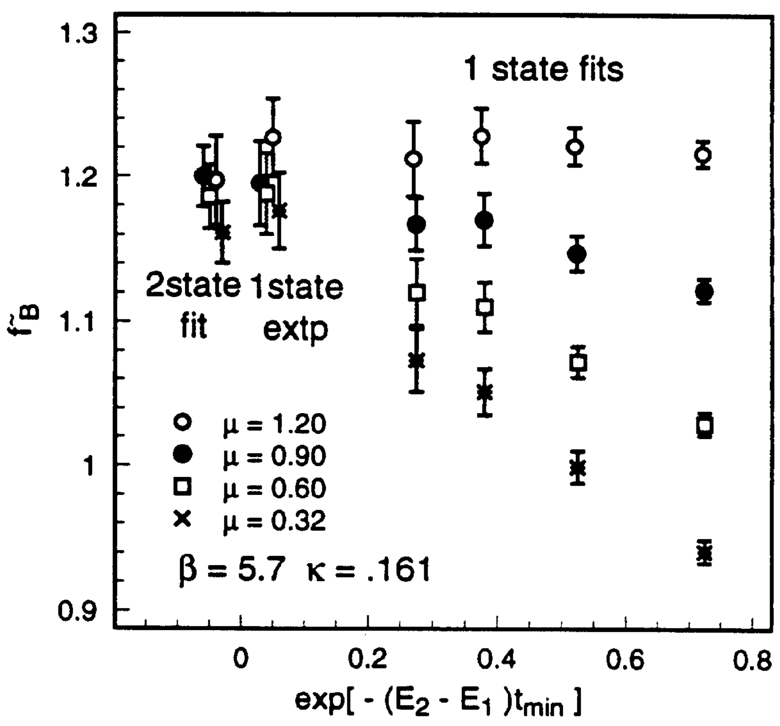

Figure 14: Time-window dependence of $\tilde{f}_B$ for 1-state fit and comparison with 2-state fit. (See caption of Fig. 13.) Also plotted for comparison are the values obtained by extrapolating the 1-state fits to $t = \infty$, using the measured value of the energy-splitting $E_2 - E_1 = 0.32$.

$(2.0fm)^3$ for $\beta = 5.7\,(12^3)$, $5.9\,(16^3)$, $6.1\,(24^3)$, and $6.3\,(32^3)$ respectively. Although these volumes appear to be comfortably large compared to the observed size of the ground state B-meson on the lattice, we consider in this section the possibility of corrections to our results due to finite volume effects and describe our method for estimating these effects. Although our overall conclusion is that these effects are negligible on the lattices considered here, the estimates discussed in this section may be useful for selecting β's and lattice sizes in subsequent studies.

An extensive theoretical study of finite volume effects on field theoretic calculations has been carried out by Luscher [45]. Consider, for example, the effect on the mass of a particle m_P. For large enough volume, the leading effect is due to the propagation of the lightest mass meson (e.g. pion) "around the world," leading to the expression for $m(L)$, the particle mass in an $L \times L \times L$ box,

$$m_P(L) = m_P(\infty) + A\frac{e^{-\lambda L}}{L} \tag{39}$$

where the exponent λ is determined by the mass of the pion, and A is given in terms of the on-shell πPP coupling. This finite volume correction can be interpreted as the effect of squeezing the pion cloud surrounding the particle. A somewhat different situation takes place when the particle P is a loosely bound state of constituents. In this case, the finite size effect is caused by the squeezing of the bound state wave function [46]. As pointed out by Luscher [47], this situation falls into the same general framework as that which led to Eq.(39), except that, in this case, the particle that travels around the world is one of the constituents of the bound state. In fact, for a nonrelativistic bound state in a non-confining potential, the finite volume effect assumes exactly the same form as (39), but in this case, the exponent λ is related to the binding energy (and hence to the spatial extent of the bound state wave function).

For the case $\beta = 5.9$ we have carried out a complete Monte Carlo investigation of the heavy-light propagators on lattices of three different sizes, $12^3 \times 24, 16^3 \times 32$, and $20^3 \times 40$ (runs e, c, and f in Table4). With the value $a^{-1} = 1.78$ GeV, these three boxes are of spatial length 1.3 fm, 1.8 fm, and 2.2 fm, respectively. The results for both the ground state energy aE_1 and for $\tilde{f}_B$ are given in Tables 7 and 8. They are seen to be the same, within errors, in all three size boxes, and thus, no significant finite size effect is observed. In order to determine an upper limit on the finite volume corrections to our results, we will make the assumption that these effects can be parametrized in the Luscher form (39).

$$aE_1(L) = aE_1(\infty) + A_{aE_1}\frac{e^{-\lambda L}}{L} \tag{40}$$

$$\tilde{f}_B(L) = \tilde{f}_B(\infty) + A_{\tilde{f}_B}\frac{e^{-\lambda L}}{L} \tag{41}$$

(Note: For particle masses in full QCD in a sufficiently large box, such an expression has been derived rigorously. For masses in quenched approximation and for decay constants, it's validity is not established, but we adopt it as a convenient ansatz. An alternative power law form is also discussed at the end of this section.) For a given choice of the exponential parameter λ, a fit to Eq. (39) gives a limit on the coefficient A.

Table 7: Volume dependence of aE_1 at $\beta = 5.9$. Results are obtained from a 2-state fit over time window $\Delta T = 3 - 10$ on lattices of size $12^3 \times 24, 16^3 \times 32$, and $20^3 \times 40$. Numbers in square brackets are the χ^2 per degree of freedom for each multistate fit.

κ	$aE_1(12)$	$aE_1(16)$	$aE_1(20)$
.154	.716(9)	.718(7)	.719(6)
	[.74]	[1.12]	[.87]
.157	.675(12)	.679(8)	.677(8)
	[.92]	[1.01]	[.62]
.158	.661(14)	.667(9)	.662(9)
	[.99]	[.92]	[.56]
.159	.652(21)	.652(12)	.641(11)
	[.98]	[.76]	[.60]
κ_c	.638(17)	.643(11)	.634(11)
	[1.01]	[.92]	[.66]

Our strategy is to extract an estimate of the exponent λ in the Luscher formula by two methods: (1) a direct study of the finite volume effects in the relativistic quark model, and (2) a study of the exponential falloff of the ground state wave function obtained in the LQCD calculation. For both $f = f_B$ and $f \overset{\sim}{=} aE_1$, the results from the RQM were calculated on $12^3, 16^3$, and 20^3 boxes. (The relativistic Van Royen-Weisskopf formula[37] was used to obtain f_B from the RQM wave function.) For the lightest quark mass studied, the RQM estimate gives $\lambda/a = 0.9$ GeV. (The results for aE_1 and for $\tilde{f}_B$ are both well fit

Table 8: Volume dependence of $\tilde{f}_B$ at $\beta = 5.9$. (See caption of Table 7.)

κ	$\tilde{f}_B(12)$	$\tilde{f}_B(16)$	$\tilde{f}_B(20)$
.154	.341(21)	.347(13)	.346(14)
.157	.299(22)	.303(14)	.298(15)
.158	.284(24)	.288(15)	.278(16)
.159	.279(35)	.271(18)	.252(17)
κ_c	.261(29)	.260(18)	.245(18)

with the same value of λ.) A slight increase in the value of λ for larger light quark mass is observed, but is inconsequential for our analysis. A direct study of the exponential falloff of the LQCD ground state wave function (using the bound state interpretation of the Luscher formula) gives a similar, but somewhat smaller estimate of $\lambda/a = 0.75$ GeV for the lightest quark mass. A smaller value of λ assumes a slower falloff with box size and thus allows for a larger finite size effect on the 16^3 and 20^3 lattices. Thus, in order to obtain a conservative upper bound on these effects, we have assumed a value $\lambda/a = 0.7$ GeV, i.e. slightly smaller than the RQM and wave function estimates. To determine the sensitivity of the conclusions to the value of λ, we also fit the data using $\lambda/a = 0.9$ GeV, which yields an upper bound on the 16^3 box about 50% smaller than the $\lambda/a = 0.7$ GeV fit. In Table 9, we give the results of fitting the $12^3, 16^3$, and 20^3 LQCD Monte Carlo results to the finite volume formula Eq. (39). For aE_1 and $\tilde{f}_B$, the Table gives the fitted infinite volume result, and an upper bound on the finite volume term evaluated on 16^3 and 20^3 lattices.

From Table 9 it is seen that, in all cases, the estimated finite volume effect on both aE_1 and on f_B is smaller than our statistical error by more than a factor of two on the 16^3 lattice and by more than an order of magnitude on the 20^3 lattice at $\beta = 5.9$. To determine the size of finite volume effects on the quantities $M_{B_s} - M_{B_d}$ and f_{B_s}/f_{B_u}, we also need to estimate the error on the slope parameters $E_1'(0)$ and f_B' in Table 6. From the κ-dependence of the finite volume fit parameters, we estimate an approximate upper bound on the finite volume error for the slopes to be $(\Delta E_1')/E_1' < .03$ and $(\Delta \tilde{f}_B')/\tilde{f}_B' < .05$ for the 16^3 box, and by $(\Delta E_1')/E_1' < .005$ and $(\Delta \tilde{f}_B')/\tilde{f}_B' < .008$ for the 20^3 box. Again this is about a factor of two below our statistics for 16^3 and entirely negligible for 20^3.

Recently, it has been argued [48] that, in intermediate ranges of volume where the

Table 9: Estimate of finite volume corrections to heavy-light results for $\beta = 5.9$. For each κ, results include the fitted infinite volume value for the ground state energy and decay constant, as well as estimated upper bounds on the finite volume corrections on 16^3 and 20^3 boxes. Unbracketed and bracketed numbers result from fitting to a Luscher asymptotic form and to a power law (L^{-3}) form, respectively.

κ	0.154	0.157	0.158	0.159	κ_c
$aE_1(\infty)$	.719(5)	.678(6)	.664(7)	.645(9)	.638(9)
	[.719(7)]	[.679(9)]	[.664(11)]	[.638(13)]	[.636(13)]
$\Delta(aE_1)(16)$	± .002	± .002	± .003	± .004	±.003
	[± .006]	[± .008]	[± .008]	[± .012]	[±.011]
$\Delta(aE_1)(20)$	± .0003	± .0004	± .0004	± .0006	±.0005
	[± .003]	[± .004]	[± .005]	[± .006]	[±.006]
$\tilde{f}_B(\infty)$	.346(11)	.300(11)	.283(12)	.257(14)	.246(14)
	[.348(16)]	[.299(17)]	[.280(19)]	[.248(23)]	[.244(21)]
$\Delta\tilde{f}_B(16)$	± .004	± .004	± .004	± .006	±.005
	[± .013]	[± .014]	[± .015]	[± .006]	[±.005]
$\Delta\tilde{f}_B(20)$	± .0006	± .0007	± .0007	± .0011	±.0008
	[± .007]	[± .007]	[± .008]	[± .011]	[±.009]

asymptotic behavior predicted by Luscher's volume formula has not yet set in, the volume dependence might be expected to exhibit a power law dependence of the form

$$m(L) = m(\infty) + \frac{const.}{L^3} \tag{42}$$

instead of the exponential falloff of Luscher's result. This power law form is also found by the authors of Ref.[48] to fit better to their data on light hadron masses (in full QCD). If we assume a similar power-law dependence for the heavy-light data, we obtain extrapolated infinite volume results and bounds on finite volume corrections which differ from those obtained with Luscher's form. The values in Table 9 which are enclosed in square brackets are the results obtained by assuming a power law dependence of the form (42). Notice that the extrapolated infinite volume values change very little compared with the previous analysis. The bound on the finite volume effects at 16^3 are somewhat larger, while those on the 20^3 lattice are much larger. However, in all cases, the bound on the finite volume effect is less than the statistical error.

To estimate finite size effects for the other β values, it is reasonable to assume approximate scaling. The box sizes for the other β's have been selected so that they are all of about the same physical size as the 16^3 box at $\beta = 5.9$ (between 1.8 and 2.0 fm). Thus, we conclude that finite size effects on all of our data is smaller than our present statistical errors. In order to quote a systematic error on our final results (see Section 6.1) for f_{B_s}/f_{B_u}, $M_{B_s} - M_{B_u}$ and f_B, we have assumed that the percentage errors for the other β values are the same as those obtained at $\beta = 5.9$ on the 16^3 box.

5.3 Extrapolation to κ_c

To investigate the sensitivity of the chirally extrapolated mass and f-values to the fitting range in κ, we have done a detailed study of the dependence of the results of the global (in κ) chi-square fit (26) on the κ values chosen, for the case $\beta = 5.9$ on a 16^3 lattice. For this run, correlators were studied at κ values of 0.154, 0.156, 0.157, 0.158, and 0.159 (with the critical κ_c =0.15975). The fits were done using a Euclidean time window $T_< = 3, T_> = 10$. By taking various subsets of κ values to perform the chiral fit (cf. discussion at end of Section(3)), we can probe the sensitivity of our results to the assumption of linearity of mass and f-values in κ^{-1}. The central values obtained from the fit (together with the associated *statistical* errors) are displayed in Table 10. The range of kappa values used in the fit is indicated in the first column using the abbreviated notation $\kappa = 0.15x \rightarrow x$ (thus: 467 indicates that the extrapolation to κ_c was made using κ values 0.154, 0.156, and 0.157).

Referring to Table 10, we see that the variation in the extrapolated ground state mass and f-value obtained by choosing three sliding windows of adjacent kappa values are in every case considerably smaller than the associated statistical errors. For the mass, the central values vary by about 50 % of the statistical error, while for the f-value the variation is 20-25 % of the statistical error. Even totally nonoverlapping fits (rows 467 and 89) give central values lying well within the statistical errors. The statistical errors of course tend to increase as we approach κ_c ; it is more difficult to detect a systematic trend in the central values because the dominant errors are statistical. For the slopes (derivatives with respect to κ^{-1}) needed for the extraction of B_s properties, the situation is similar. Aside from the 89 fit, which gives a poor determination of the slopes, the central values for all the subsets of κ's are well within a standard deviation of the full fit to all five kappa values.

We may conclude from the preceding that, as in the case of finite volume corrections,

Table 10: Estimate of systematic effects in chiral extrapolation. Listed are the values at κ_c and slopes (as a function of $\kappa^{-1} - \kappa_c^{-1}$) of the ground state energy and decay constant obtained from a fit to subsets of the five κ values, .154, .156, .157, .158, and .159. First column indicates the set of κ's used by listing the last digit of each κ included.

κ range	$E_1(0)$	$E_1'(0)$	$\tilde{f}_B(0)$	$\tilde{f}_B'(0)$	χ^2/dof
467	.643(10)	.319(22)	.464(29)	.689(68)	1.03
678	.645(10)	.303(36)	.463(29)	.698(110)	0.96
789	.642(13)	.332(72)	.458(36)	.744(202)	0.87
89	.640(15)	.385(123)	.453(41)	.832(346)	0.84
6789	.643(12)	.321(52)	.459(33)	.725(146)	0.89
46789	.643(11)	.320(33)	.460(31)	.700(95)	0.92

nonlinearities in the chiral extrapolation are not an important source of systematic error in our results. In order to arrive at an actual estimate of the chiral extrapolation contribution to the total systematic error we have taken the variation in the 3-kappa fits in Table(10) (i.e rows labelled 467,678, and 789) which have a reasonable lever arm in $1/\kappa$, and fairly small statistical errors, as an indication of the extrapolation error to κ_c (i.e. in f_{B_u} and M_{B_u}). As we measure quite close to κ_s (at κ =0.157), there is effectively no extrapolation error in the strange quark quantities. We assume that the chiral extrapolation at β=5.9 is typical of other β values. In this way a chiral extrapolation part of the total systematic errors quoted in Section 6.1 can be obtained.

5.4 Scale Errors

In order to quote physical values of masses and decay constants, one must select a particular dimensionful quantity to define the scale. In our discussion, we have taken the values of a^{-1} obtained from the 1P-1S charmonium splitting[43] at $\beta = 5.7, 5.9$, and 6.1. Our choice of a^{-1} at $\beta = 6.3$ is obtained by evolving from $\beta = 6.1$ via one-loop asymptotic freedom. (The same value of $a^{-1} = 3.08$ is also obtained from our value for m_ρ.) Other possible choices for the scale-defining parameter include string tension, rho mass, and f_π. Since the quoted values of the decay constant f_B include a factor of $a^{\frac{3}{2}}$, it is particularly important to estimate the possible systematic error in our results arising from uncertainty in the overall scale at each β value. In Fig. 15 we have plotted the scale obtained from m_ρ (circles and filled circles), f_π (squares), and string tension (diamonds and filled diamonds) relative to the scales chosen in this paper (Table 1). Also included on the plot are points (filled squares) obtained from lattice calculations of the deconfinement temperature T_c [38]. Since the experimental value of T_c is not known, these calculations only give a relative determination of the scale at different β's. (The absolute scale for these points has been chosen to be equal to that in Table 1 at $\beta = 6.3$, which corresponds to a deconfinement temperature of $kT_c = 264$ MeV.) The values for m_ρ are from GF11 [40] (filled circles) and from our data (Table A)(circles), while the string tension is a combination of our results at 5.7, 5.9, and 6.1 (diamonds) and those of Ref. [39] at 6.0, 6.2, and 6.4 (filled diamonds). For the latter points, the charmonium scales were estimated from Table 1 by linear interpolation in ln a. The values for f_π are taken from Table A.

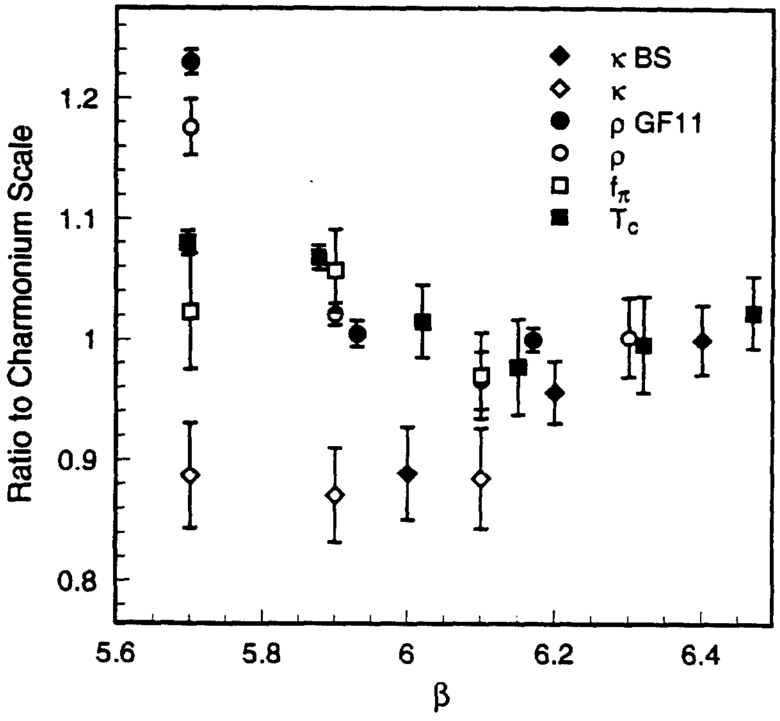

Figure 15: Scales obtained from m_ρ (circles and filled circles), f_π (squares), string tension (diamonds and filled diamonds), and deconfinement temperature T_c (filled squares) relative to the scales in Table 1. Our data is denoted by open symbols.

The trend exhibited by the data in Fig. 15 indicates a significant scale discrepancy in the range $\beta = 5.7$ to 6.0, with the m_ρ scale being about 10-20% higher and the string-tension scale about 10-15% lower than charmonium. For $\beta \geq 6.2$, the scales appear to converge to much better agreement, with deviations of $\leq 5\%$. This suggests that much of the discrepancy at lower β is due to finite lattice spacing effects, as opposed to being an effect of the quenched approximation. (Discrepancies which do not go away in the scaling limit can be ascribed to the neglect of closed quark loops.) The data shown in Fig. 1 illustrates that, over the entire range of β, the charmonium scale differs little from a weighted average of the other choices. This provides some additional confidence in our choice of scales. To estimate the scale error on our heavy-light results, we have used the charmonium scale errors quoted in Ref. [43] (which include both statistics and systematics). For $\beta = 6.3$ we have taken a conservative scale error estimate of 5%, based on the spread of values shown in Fig. 15.

Our final results for $M_{B_s} - M_{B_u}$ and f_{B_u} (f_{B_s}/f_{B_u} is dimensionless) quoted below are therefore subject to a 5% and 7% error (resp.), assuming that continuum extrapolated objects are determined primarily by the larger β values where the scale discrepancy is small. The larger error for f_B arises from the fact that the quantity computed on the lattice scales like $a^{3/2}$.

5.5 Extrapolation to the continuum

By far the largest systematic error in our calculations arises in the extrapolation of the f_B results to zero lattice spacing. In comparison, the systematic errors incurred from working on a finite volume lattice, at finite light quark mass, or even (very probably) the neglect of quark loops are negligible. The difficulties here are both intrinsic and practical. On the one hand, the detailed form of the lattice spacing dependence of lattice quantities is generally rather complicated (involving logarithmic as well as power dependence on the lattice spacing), in contrast to the relatively well understood structure of the chiral or finite volume extrapolations. On the other hand, reduction of the lattice spacing by a factor of 2 requires increasing the lattice volume 16-fold (if we maintain fixed physical space-time volume).

These issues are particularly important in the case of heavy meson decay constants. We find that the lattice spacing dependence for f_B in the static limit is considerably stronger

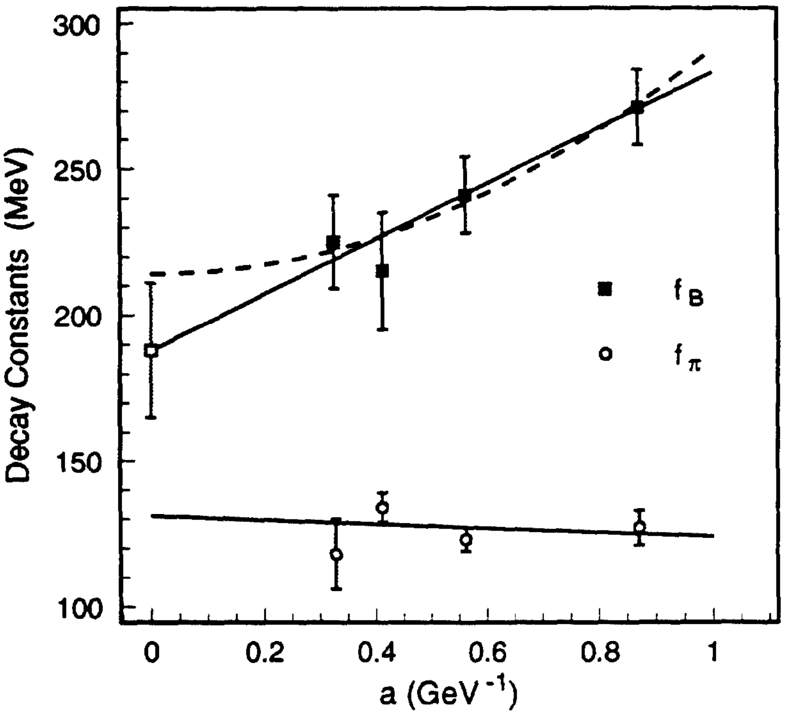

Figure 16: f_B at $\kappa = \kappa_c$ as a function of lattice spacing. The scales and renormalization constants used are given in Table 1. The solid line is the best linear fit. The dashed line is a quadratic (a^2) fit used to estimate systematic error in $a \to 0$ extrapolation. (See Section 5.5)

than for f_π. This is illustrated in Fig. 16. Although our calculations have led to reasonably precise results at finite a, quoting a systematic error on the continuum extrapolated result clearly requires an investigation of the variation induced by alternative fitting procedures.

Table 11: Comparison of continuum values for a linear vs. a quadratic fit to the a-dependence of physical quantities. Values shown are the fitted $a = 0$ values of $f_B, M_{B_s} - M_{B_u}$, and f_{B_s}/f_{B_u}, and the χ^2 per degree of freedom for each fit. Errors shown are extrapolated statistical errors.

fit	$f_B(MeV)$	χ^2/dof	$M_{B_s} - M_{B_u}$	χ^2/dof	f_{B_s}/f_{B_u}	χ^2/dof
$c_0 + c_1 a$	188(23)	.46/2	86(12)	2.4/2	1.22(4)	2.4/2
$c_0 + c_1 a^2$	214(13)	.40/2	80(7)	2.3/2	1.21(2)	2.2/2

We have investigated this variation by fitting the f_B results at finite β to various functional forms for the finite a correction. In Table 11 we show the extrapolated continnum result for f_B and the χ^2 per degree of freedom for the alternatives that the finite lattice spacing correction is of order a and of order a^2. The linear and square fits are, explicitly,

$$f_B(a) = 188(23)\,(1 + .51(19)a) \text{ MeV} \tag{43}$$

$$f_B(a) = 214(13)\left(1 + [.60(11)a]^2\right) \text{ MeV} \tag{44}$$

where a is in GeV^{-1}. For $M_{B_s} - M_{B_u}$, the fits are

$$M_{B_s} - M_{B_u}(a) = 85.8(11.7)\,(1 - .24(22)a) \text{ MeV} \tag{45}$$

$$M_{B_s} - M_{B_u}(a) = 80.1(6.7)\left(1 - [.47(40)a]^2\right) \text{ MeV} \tag{46}$$

and

$$f_{B_s}/f_{B_u}(a) = 1.216(41)\,(1 - .02(6)a) \tag{47}$$

$$f_{B_s}/f_{B_u}(a) = 1.213(23)\left(1 - [.16(31)a]^2\right) \tag{48}$$

These fits are shown with the data in Fig. 16. It is clear from this graph that it would be very difficult to distinguish between these two possibilities by calculations in the range $\beta = 5.7 - 6.3$, even with improved statistics and additional β values. In the absence of more precise data at much larger β or a complete control of all $O(a)$ lattice effects, we will take the variation of the extrapolated results in Table 11 as an estimate of the systematic error associated with extrapolating to $a = 0$. In our final result for f_B, we quote the continuum value obtained from the linear fit with asymmetric errors of +26 and -0 to allow for this extrapolation uncertainty.

6 Physical Results and Discussion

6.1 Final results

In this final section, we collect our results for f_{B_s}/f_{B_u}, $M_{B_s} - M_{B_u}$, and f_{B_u} at each lattice spacing calculated and then present the results extrapolated to the continuum. The summary of results for each of the four lattice spacings studied are collected in Table 12. A comparison with other recently reported results follows immediately. In all cases the first error quoted is a statistical error obtained by the jackknife procedure described previously.

Table 12: Final results at fixed β (lattice spacing) for f_B, $M_{Bs} - M_{Bu}$, and f_{Bs}/f_{Bu} in the static approximation. The first error is statistical and the second is systematic.

β	f_B(MeV)	$M_{B_s} - M_{Bu}$(MeV)	f_{Bs}/f_{Bu}
5.7	$271 \pm 13 \pm 20$	$66 \pm 7 \pm 6$	$1.181 \pm .030 \pm .012$
5.9	$241 \pm 13 \pm 13$	$74 \pm 5 \pm 6$	$1.211 \pm .018 \pm .014$
6.1	$215 \pm 21 \pm 14$	$87 \pm 9 \pm 7$	$1.226 \pm .027 \pm .016$
6.3	$225 \pm 17 \pm 14$	$68 \pm 10 \pm 5$	$1.172 \pm .031 \pm .011$

The source of systematic errors varies somewhat with the quantity being computed. For f_{B_s}/f_{B_u}, the uncertainty in the scale cancels, as the ratio is a dimensionless quantity. Thus, for this quantity, the quoted systematic error includes finite volume and chiral extrapolation errors. The lattice spacing dependence of this quantity (see Fig(7)) is very small, so we have not included a continuum extrapolation error. The result is

$$f_{B_s}/f_{B_u} = 1.216 \pm 0.041(\text{stat}) \pm 0.016(\text{syst}) \tag{49}$$

For the mass splitting $M_{B_s} - M_{B_u}$ the systematic errors include finite volume effects, the chiral extrapolation (to determine M_{B_u}), and an estimate of the scale error. For the continuum extrapolation, we quote the result obtained from the linear fit in a, and take the difference between the two fits shown in Table 11 as an estimate of our extrapolation error (+0 to −6). Combining the extrapolation error with our other systematic errors, we obtain the result

$$M_{B_s} - M_{B_u} = 86 \pm 12(\text{stat})\ ^{+7}_{-9}(\text{syst})\ \text{MeV}. \tag{50}$$

Finally, for f_B itself, there is, in addition to the usual finite volume and chiral extrapolation errors, a substantial (not necessarily linear) lattice spacing dependence, as well as the possibility of sizable renormalization corrections to Z at the two and higher loop level. These additional systematic errors are quoted separately in our final result:

$$f_{B_u} = 188 \pm 23(\mathrm{stat}) \pm 15(\mathrm{syst})\, {}^{+26}_{-0}(\mathrm{extrap}) \pm 14(\mathrm{renorm})\ \mathrm{MeV}. \tag{51}$$

6.2 Comparison with other results

There have been several recently reported studies of the heavy-light meson system in the static limit of quenched LQCD. In this Section we will assess the results reported here in comparison with these other studies. We will consider four quantities, E_1, the heavy-light ground state energy, the $M_{B_s} - M_{B_u}$ mass splitting, f_B the ground-state decay constant, and the ratio f_{B_s}/f_{B_u}. Even before the present study, there has been some apparent disagreement among different groups over the size of f_B. Some of these discrepancies can be traced to different choices of β and κ, different definitions of the QCD length scale, and different evaluations of the perturbative renormalization constant Z. Since our data has provided a more accurate determination of the dependence on κ and β, we are able to interpolate our data in both variables and make a direct comparison with other groups.

The focus of this subsection is on the lattice measurement of the ground state energy eigenvalue E_1 and its matrix element with the unrenormalized local axial current operator on the lattice, $\tilde{f}_B = v_1^N$ (c.f. Eq.(22)). These are the quantities that are extracted directly from the lattice heavy-light meson propagators and, for given β and κ, are independent of the choices for length scale and renormalization constant.

First consider the ground state energy E_1. In Section 4.1 it was shown that the κ and a dependence of E_1 is most easily described by introducing the naive quark mass $m_q = (2\kappa a)^{-1} - (2\kappa_c a)^{-1}$. The values of κ_c for $\beta = 5.74$ and 6.26 are taken from [14] while that at $\beta = 6.0$ is taken from [12]. The κ_c values for $\beta = 5.7, 5.9, 6.1$, and 6.3 are from our own data. The values for the scale a^{-1} are subject to somewhat more uncertainty. For 5.7, 5.9, 6.1, and 6.3, the scales we have used are given in Table 1. In order to have a reasonably self-consistent set of scales, the remaining values for a^{-1} are obtained from those at 5.7, 5.9, and 6.1 by a simple linear interpolation or extrapolation in $\ln a$. Note that we are only using the value of a^{-1} here to define the naive quark mass m_q. The numerical values of E_1 and $\tilde{f}_B$ are obtained directly from the lattice propagators and do not depend on choice of scale. Thus, our comparison of data is insensitive to an overall, uniform change of scales. The

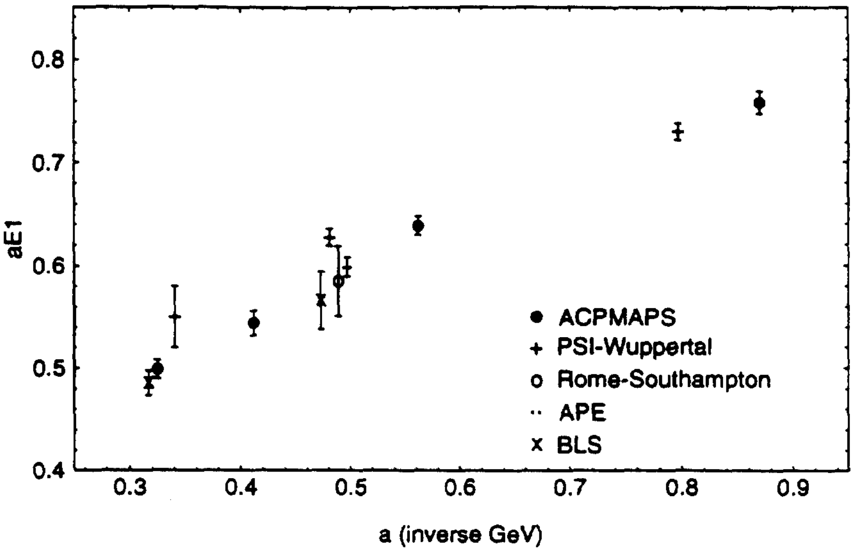

Figure 17: Ground state energy, in lattice units, at $\kappa = \kappa_c$, versus lattice spacing. Points at the same a have been slightly displaced for readability.

values for the ground state energy E_1 (in lattice units), extrapolated to κ_c, from the various studies are plotted in Fig.17. We conclude from these plots that all the data are in reasonable agreement, both on the magnitude of E_1 and on its a dependence. This is not surprising since, for any reasonably well-chosen smearing function, the value of E_1 is obtained fairly unambiguously from the smeared-smeared correlator. Our multistate analysis provides a value of E_1 with considerably smaller errors than a single-channel analysis (note the much smaller error bars for the ACPMAPS results), but the results are completely consistent with previous calculations.

Results from various groups for the $M_{B_s} - M_{B_u}$ splitting are compared with ours in Fig 18. Again, the accurate determination of the slope of the ground state energy with respect to $1/\kappa$ is the key to the much smaller error bars shown for the ACPMAPS results. However, the results are basically consistent within errors. For this quantity, the lattice spacing dependence is very mild.

Results from various groups for the ratio of decay constants f_{B_s}/f_{B_u} are compared with ours in Fig 19.

In contrast with the situation for E_1 or $M_{B_s} - M_{B_u}$, there is significant disagreement on the value of $\tilde{f}_B$ among the various studies, even after correcting for the different values of κ

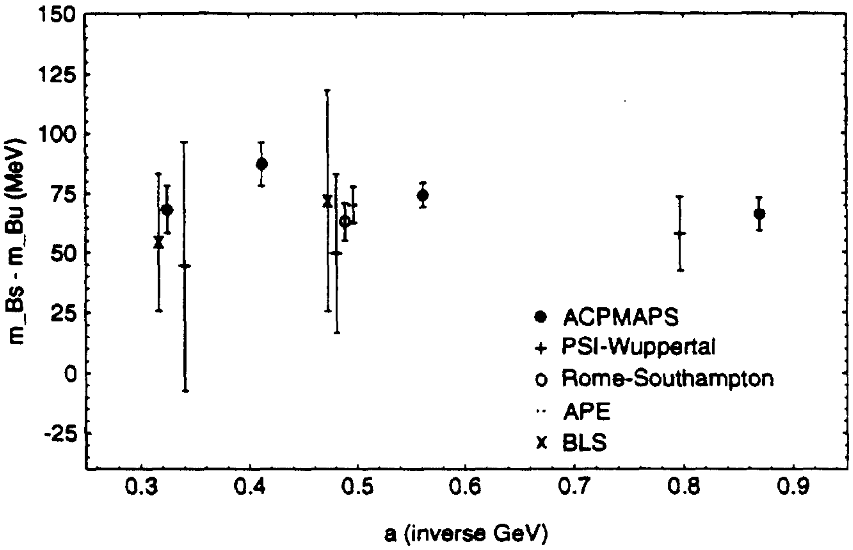

Figure 18: Mass splitting, $M_{B_s} - M_{B_u}$, in physical units, versus lattice spacing. Points at the same a have been slightly displaced for readability.

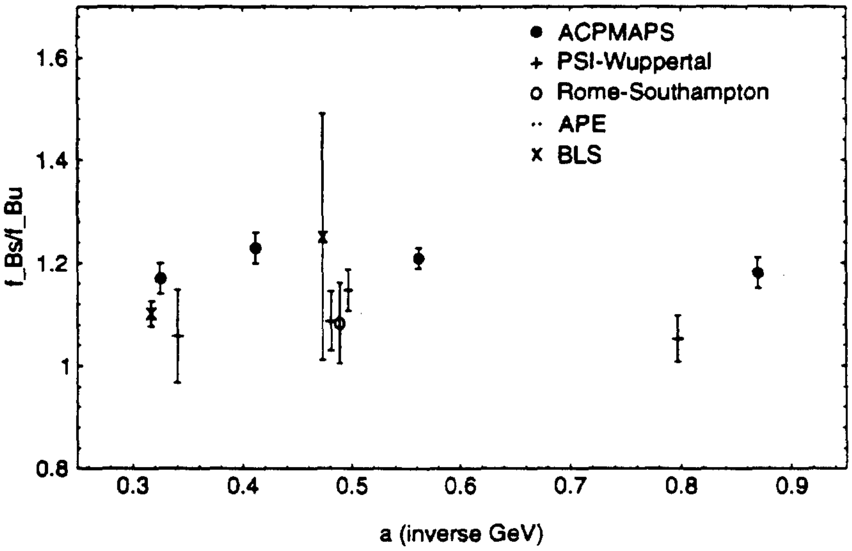

Figure 19: Comparison of f_{B_s}/f_{B_u} vs. lattice spacing for present results and other recent works. Points at the same a have been slightly displaced for readability.

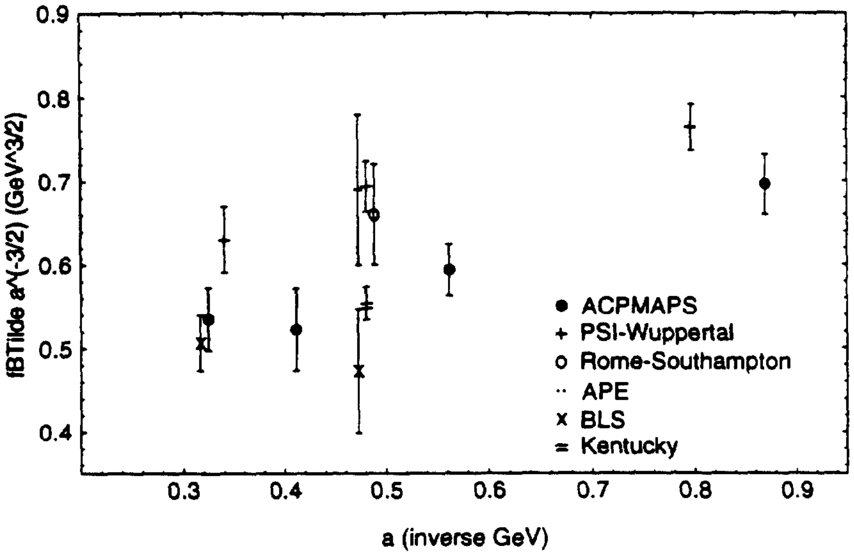

Figure 20: Comparison of $\tilde{f}_B$ vs. lattice spacing for present results and other recent works. Points at the same a have been slightly displaced for readability.

and β. Results from references [44, 41, 12, 14, 49] are compared with our data in figure 20. This is a plot of $\tilde{f}_B a^{-3/2}$ against lattice spacing a, so that we can compare 'raw' lattice results without renormalisation factors. The results of [12] (at $\beta = 6.3$) and [49] are in good agreement with ours, while [44, 41, 14] report substantially larger values.

We believe that the discrepancies can be traced primarily to the incomplete isolation of the ground state with the sources chosen. Observe in particular that the result in [49], where a variational method is used to isolate the ground state, is in good agreement with us. Sensitivity of the apparent value of f_B to the form of the source has been emphasized in [50].

6.3 Future Studies

We have presented results for the decay constant f_B and for masses of low-lying heavy-light states in the static approximation. The analysis procedure introduces several improvements over previous smearing methods. First, the success of the RQM in reproducing the measured lattice wave functions is exploited by using the RQM to construct not only an accurate ground state wave function, but also a set of orthonormal excited state smearing functions. Second, we make full use of the information contained in the matrix of smeared-smeared and smeared-local correlators, including both ground state and excited state smearing functions at each end. Our method provides much greater control over systematic errors from higher state contamination, because of the fact that the source smearing functions are tuned directly to the lattice wave functions, without regard to the behavior of the effective mass plots. The appearance of long plateaus in the SS and SL plots at the same value of effective mass is thus strong evidence that the systematic error from higher states has been largely eliminated. We will report the application of our methods for heavy-light mesons to the spectrum of radial and orbital excitations for heavy-light systems and the B parameter in forthcoming papers.

We expect to be able to improve the accuracy of the present results for the $M_{B_s} - M_{B_u}$ and f_{B_s}/f_{B_u} by using larger ensembles. There are two other sources of systematic uncertainty in our results for f_B. Use of the Wilson action for the light quarks implies lattice spacing corrections in O(a) and the large one loop renormalization for the axial current suggests that the two loop correction may be sizable. Study of these effects will be required to substantially improve the error on f_B.

A Light Hadron Results

In this Appendix we report the results for the light quark sector which we have used to set the parameters for the heavy-light meson properties. First consider the light-light pseudoscalar meson mass as a function of the light quark hopping parameters. This serves to determine the critical hopping parameter at each value of β studied. Using the physical K mass, we also establish the correct hopping parameter for the strange quark. (The small effect from the nonzero up or down quark mass has also been included in our results.) In addition to determining the light quark hopping parameters from the pseudoscalar meson masses, the meson propagators have also been analyzed to obtain the values of f_π and m_ρ. All of the results discussed here for the light hadron parameters have been extracted from local $q\bar{q}$ operators. An analysis of light meson parameters using smeared sources in Coulomb gauge is in progress and will be reported elsewhere.

Let the hopping parameters for the two valence quarks in the light meson be denoted by κ_1 and κ_2, and denote the pseudoscalar meson mass by m_P. All of our data is consistent with a linear dependence of m_P^2 on κ_1^{-1} and κ_2^{-1}. The results can be expressed in terms of the parameters C and κ_c of the linear fit

$$(m_P a)^2 = C\left(\kappa_1^{-1} + \kappa_2^{-1} - 2\kappa_c^{-1}\right) \tag{52}$$

The results for the four β values studied are given in Table 13. Using the scales in Table 1, the naive quark masses, defined by

$$m_q = \frac{1}{2\kappa a} - \frac{1}{2\kappa_c a} \tag{53}$$

are also listed in Table 13. (Here, up and down quarks are taken to be degenerate in mass.) A plot of m_P^2 vs. quark mass (defined in Eq. (53)) is shown in Fig. 21. For $\beta = 5.7, 6.1$, and 6.3 the values of $m_P a$ were obtained using equal quark masses, $\kappa_1 = \kappa_2$. For $\beta = 5.9$ several combinations of unequal quark mass values (open circles in Fig.21) were used to check the validity of Eq.(52). For $\beta = 5.9$, in addition to the main run on a $16^3 \times 32$ lattice, in order to investigate finite volume effects, we have also carried out Monte Carlo runs on $12^3 \times 24$ and $20^3 \times 40$ lattices. The results labeled 5.9(∞) are the infinite volume values obtained by fitting all three box sizes to the functional form derived by Luscher, as discussed in Sec. 5.2.

In Table 13, the values for C and κ_c are independent of the scale chosen for a^{-1}. The

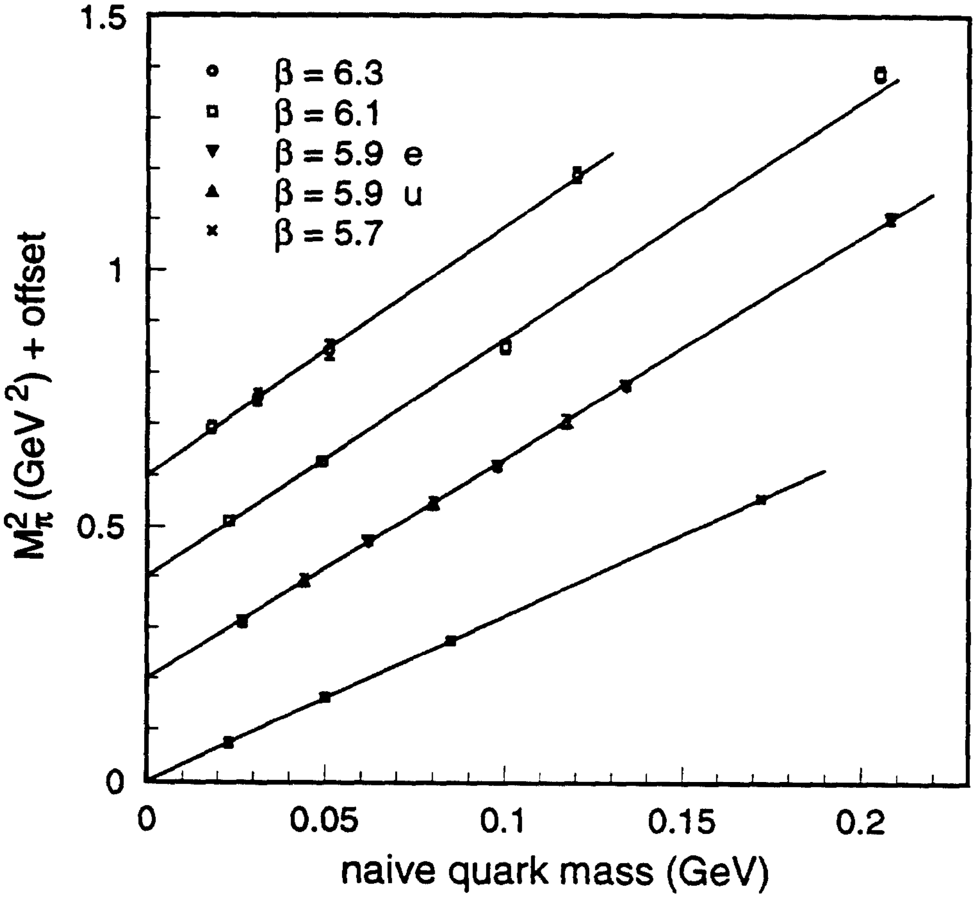

Figure 21: m_π^2 vs. naive quark mass for $\beta = 5.7, 5.9, 6.1$, and 6.3. The vertical scales for 5.9, 6.1, and 6.3 are offset by multiples of 0.2 for display purposes. Points labeled 5.9e and 5.9u represent mesons with equal and unequal quark masses, respectively. Values with unequal quark mass are plotted at the average mass $(m_1 + m_2)/2$

Table 13: Light quark hopping parameters obtained from light pseudoscalar meson mass measurements. Values are shown for each run, as well as the infinite volume extrapolated value at $\beta = 5.9$. C is the slope of the pseudoscalar $(\text{mass})^2$ as a function of κ^{-1}. The last two columns give the strange and up quark masses $\times 2a$. Errors are statistical.

Run	β	κ_c	C	$\kappa_s^{-1} - \kappa_c^{-1}$	$\kappa_u^{-1} - \kappa_c^{-1}$
b	5.7	.16914(10)	.703(10)	.2533(36)	.01024(15)
e	5.9	.15972(14)	.615(14)	.1209(27)	.00489(11)
c	5.9	.15975(6)	.609(9)	.1221(18)	.00494(7)
f	5.9	.15981(4)	.591(8)	.1258(17)	.00509(7)
	5.9(∞)	.15980(4)	.597(7)	.1245(14)	.00504(6)
d	6.1	.15496(3)	.480(11)	.0832(19)	.00336(8)
g	6.3	.15178(4)	.395(10)	.0613(15)	.00248(6)

remaining columns are computed using the scales in Table 1. The errors quoted in Table 13 are statistical only, and do not include the uncertainty associated with the choice of a^{-1}. The uncertainty arising from the scale determination, along with other sources of error, will be discussed in Section 6.

Although they are not used in the body of the paper, we also briefly discuss our results for the rho mass and the pion decay constant. We again emphasize that all of the results discussed here are obtained from light quark propagators with δ-function sources. The results are thus subject to possible systematic errors from higher state contamination. This is not a problem in measuring the pion and kaon masses discussed above, but it becomes more of a difficulty for m_ρ and f_π measurements. In order to determine f_π, one must calculate both the propagator with a pseudoscalar ($\bar{q}\gamma_5 q$) source at each end (PP), and the propagator with a pseudoscalar source at one end and an axial vector ($\bar{q}\gamma_5\gamma_0 q$) source at the other end (PA). (Note: One may also use the (AA) propagator with an axial vector source at both ends. However, since the vacuum to one pion matrix element of the axial vector source contains an explicit factor of m_π, the pion pole residue in the (AA) propagator vanishes more rapidly than that of the (PA) propagator in the chiral limit, making it more difficult to measure accurately.) The (PP) and (PA) propagators are fit to a single exponential in the time ranges shown. Table A summarizes our results for light hadron parameters. Again,

Table 14: Results for light-light mesons. Meson propagators were fit to a single exponential over time window ΔT. Result for f_π includes a tadpole improved renormalization factor, computed in Ref.[20].

β	ΔT	κ	$m_\pi a$	$m_\rho a$	$f_\pi a$
5.7	6-10	.161	.649(3)	.787(2)	.145(3)
		.165	.456(5)	.675(5)	.133(4)
		.1667	.351(8)	.629(15)	.115(6)
		.168	.237(13)	.586(44)	.102(11)
		κ_c	0	.566(11)	.108(14)
5.9	8-12	.154	.527(2)	.619(2)	.104(2)
		.156	.426(3)	.546(3)	.093(2)
		.157	.360(2)	.513(3)	.086(2)
		.158	.288(3)	.479(5)	.078(2)
		.159	.195(4)	.444(12)	.072(4)
		κ_c	0	.418(4)	.067(2)
6.1	10-16	.151	.409(3)	.482(3)	.081(2)
		.153	.276(4)	.401(4)	.069(2)
		.154	.196(3)	.361(8)	.061(2)
		.1545	.137(5)	.341(19)	.056(4)
		κ_c	0	.324(8)	.055(2)
6.3	12-18	.1500	.249(3)	.331(3)	.054(2)
		.1510	.160(6)	.283(5)	.045(4)
		.1513	.126(6)	.269(7)	.041(4)
		.1515	.099(5)	.260(11)	.038(11)
		κ_c	0	.246(8)	.037(3)

Table 15: Light-light meson results at $\beta = 5.9$ for lattice sizes $12^3 \times 24(e)$, $16^3 \times 32(c)$, and $20^3 \times 40(f)$. Result for f_π includes the tadpole improved renormalization factor, computed in Ref. [20].

β	ΔT	κ	$m_\pi a$	$m_\rho a$	$f_\pi a$
5.9(e)	8-12	.154	.535(4)	.618(4)	.105(3)
		.157	.364(4)	.505(7)	.083(4)
		.158	.306(9)	.475(15)	.080(4)
		.159	.198(33)	.375(77)	.075(17)
		κ_c	0	.403(14)	.067(5)
5.9(c)	8-12	.154	.534(3)	.622(2)	.106(3)
		.157	.364(4)	.508(5)	.087(3)
		.158	.292(4)	.469(8)	.079(4)
		.159	.188(8)	.440(27)	.067(8)
		κ_c	0	.407(8)	.067(4)
5.9(f)	8-12	.154	.525(2)	.617(2)	.103(2)
		.157	.358(3)	.515(4)	.085(2)
		.158	.288(3)	.482(5)	.078(3)
		.159	.196(4)	.442(12)	.073(4)
		κ_c	0	.423(5)	.068(2)

the errors quoted are purely statistical. Some systematic errors are expected particularly for f_π, for which a stable mass plateau in the (PA) propagator with the same mass as the (PP) propagator was not generally achieved. An attempt was made to compensate for this by fitting the (PA) propagator with the mass fixed to be equal to that of the (PP) propagator. It is clear from these results that a much better determination of f_π from our data will be possible when smeared operators are employed. The rho propagators exhibit reasonable plateaus in the time intervals shown in Table A, but a study of the variation of the results with different ΔT windows indicates that a systematic error of from 1 to 2 times the statistical errors cannot be ruled out. The values of $f_\pi a$ given in Table A include the perturbative renormalization constants computed in Ref. [20]. For $\beta = 5.9$, the results in Table A are the infinite volume extrapolated results from the three Monte Carlo runs on 12^3 (e), 16^3 (c), and 20^3 (f) boxes (except for $\kappa = .156$ which was done only on the 16^3 box). The results on each size box are listed separately in Table A. In the main analysis of this paper, the only light meson parameters we will use are the hopping parameters determined from the pseudoscalar masses. Since the (PP) propagator always exhibits a stable mass plateau, these parameters are well-determined and should be relatively free of systematic error from higher states.

B Multistate Extraction of Meson Wavefunctions

A particularly graphic illustration of the power of the smearing technique in reducing the contamination of higher states is obtained by examining the time development of the Coulomb gauge Bethe-Salpeter wavefunction of a static-light meson beginning with either (a) the RQM smeared source defined in equation (17), or (b) a cube smeared source [41]. In the first case, we extract

$$\Psi_{BS}(R,T) \equiv < 0|q(R,T)\bar{Q}(0,T)|\Phi^{(a)},0 > \tag{54}$$

for the ground state (a=1) at small Euclidean times. We have done the comparison for the case β =5.9, κ =0.159, on a 16^3 lattice. In Fig.22 the evolution of the wavefunction using a source smeared with the ground state wavefunction of the RQM (with constituent mass μ=0.12) is shown for Euclidean times T=1,2 and 4. It is apparent that the wavefunction has reached its asymptotic value to very good accuracy already at time slice 2, with little further change at T=4 (in fact, the overlap of the wavefunction at T=2 with that at T=4 is 0.9986!). In Fig.23 the corresponding evolution (again for Euclidean times T=1,2 and 4) is shown for a source smeared over a cube of width 7 lattice spacings. Here the convergence is much slower, with the pointwise convergence near the origin particularly tardy.

Although the use of a single smearing function obtained from the RQM is adequate to the task of extracting the ground-state Bethe-Salpeter wavefunction, even the improved smearing given by the RQM is not sufficient if we wish to do the same for the higher excited states in a given channel. In Section 4 we showed how to define optimized smeared states $| \hat{\Phi}^A >$ in which the admixture of all but one (the A'th) of the first M meson states in a given channel is tuned to zero. For example, taking M=3 at β=5.9, κ=0.159 on a 16^3 lattice, one finds that the choice of smearing function (cf. Sect 3.2,Eq (23))

$$| \hat{\Phi}^{(2)} >= 0.03 \mid \Phi^{(1)} > +0.82 \mid \Phi^{(2)} > +0.57 \mid \Phi^{(3)} > \tag{55}$$

produces an optimized first excited state in the sense that admixtures of the ground and second excited state are tuned out (based on a fit of the form (22)) with $T_<$=2,$T_>$=7). The use of such an optimized smearing is crucial if we wish to extract the correct Bethe-Salpeter wavefunction of the first radial excited state near the origin. Any sizable admixture of the exact meson ground-state will otherwise dominate the small r region of the wavefunction at large Euclidean time, *before* the higher (2nd, 3rd,etc) states have decayed away. In Figure

24 we show this phenomenon with a Bethe-Salpeter wavefunction $\Psi_{BS}(R,T)$ defined as

$$\Psi_{BS}(R,T) \equiv < 0 \mid q(\vec{R},T)\bar{Q}(0,T) \mid \Phi^{(2)},0 > \tag{56}$$

The wavefunction (renormalized to unit norm) is plotted for Euclidean times T=1,2,4, and 6. There is a steady upward drift of the wavefunction at the origin as T increase to 4, but by time slice 6 the influence of the ground state is clearly apparent as the latter begins to dominate the evolved meson state. It would clearly be very difficult to draw any firm conclusions about the behavior of the excited state wavefunction close to the origin from these measurements.

On the other hand, using the optimized smearing found above (55), and computing

$$\Psi^{\rm opt}_{BS}(R,T) \equiv < 0 \mid q(\vec{R},T)\bar{Q}(0,T) \mid \hat{\Phi}^{(2)},0 > \tag{57}$$

one finds (Fig.25 shows the optimized wavefunction for times T=1,2,3) a rapid convergence to an asymptotic shape by the *third* time slice, giving a value for the wavefunction at the origin $\simeq$0.44, as compared to a maximal value $\simeq$0.36 obtained at T=4 from Eq (56) before convergence is lost. Eventually, of course, the ground state will dominate in this case also, but by using the optimized state, we correctly extract the exact Bethe-Salpeter wavefunction for the excited state before the ground state contamination has a chance to become sizable.

ACKNOWLEDGEMENTS

The authors wish to acknowledge the contributions of Aida El-Khadra to this work. We have also thank Andreas Kronfeld and Paul Mackenzie for valuable discussions. JMF thanks the Nuffield Foundation for support under the scheme of Awards for Newly Appointed Science Lecturers. BRH was supported in part by the Department of Energy under Grant No. DE–FG03–91ER 40662, Task C. HBT was supported in part by the Department of Energy under Grant No. DE-AS05-89ER 40518. AD was supported in part by the National Science Foundation under Grant No. PHY-90-24764. This work was performed using the ACPMAPS computer at the Fermi National Accelerator Laboratory, which is operated by Universities Research Association, Inc., under contract DE-AC02-76CHO3000.

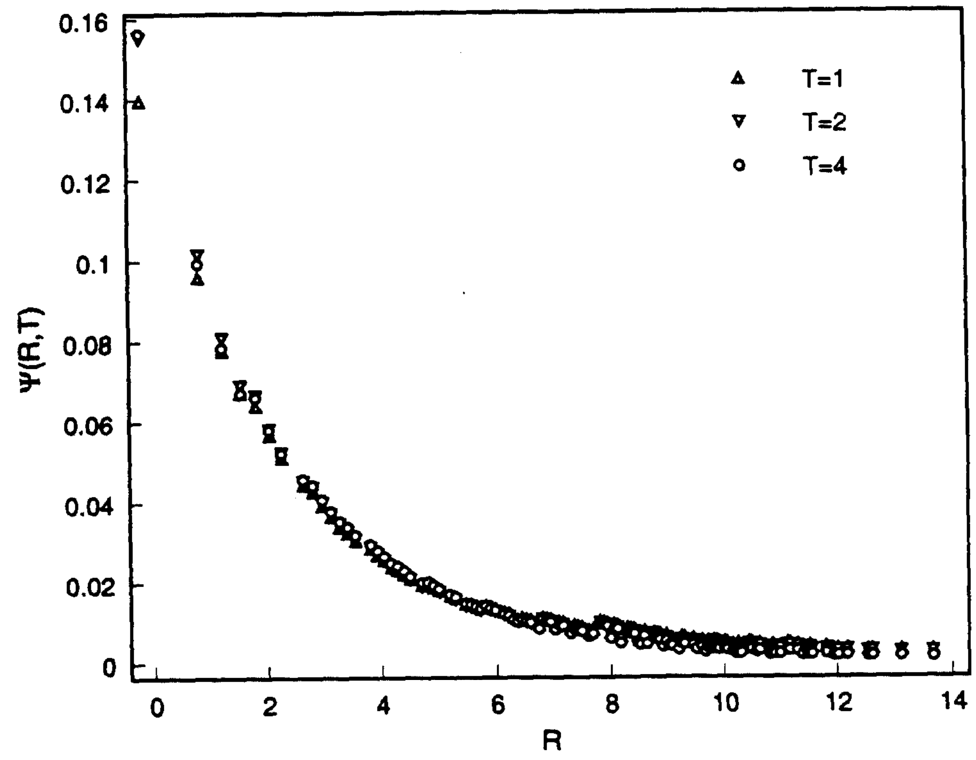

Figure 22: Time evolution of the ground state heavy-light wavefunction for $\beta = 5.9, \kappa = .159$, using a source smeared with the ground state wavefunction of the RQM with constituent mass parameter $\mu = 0.12$.

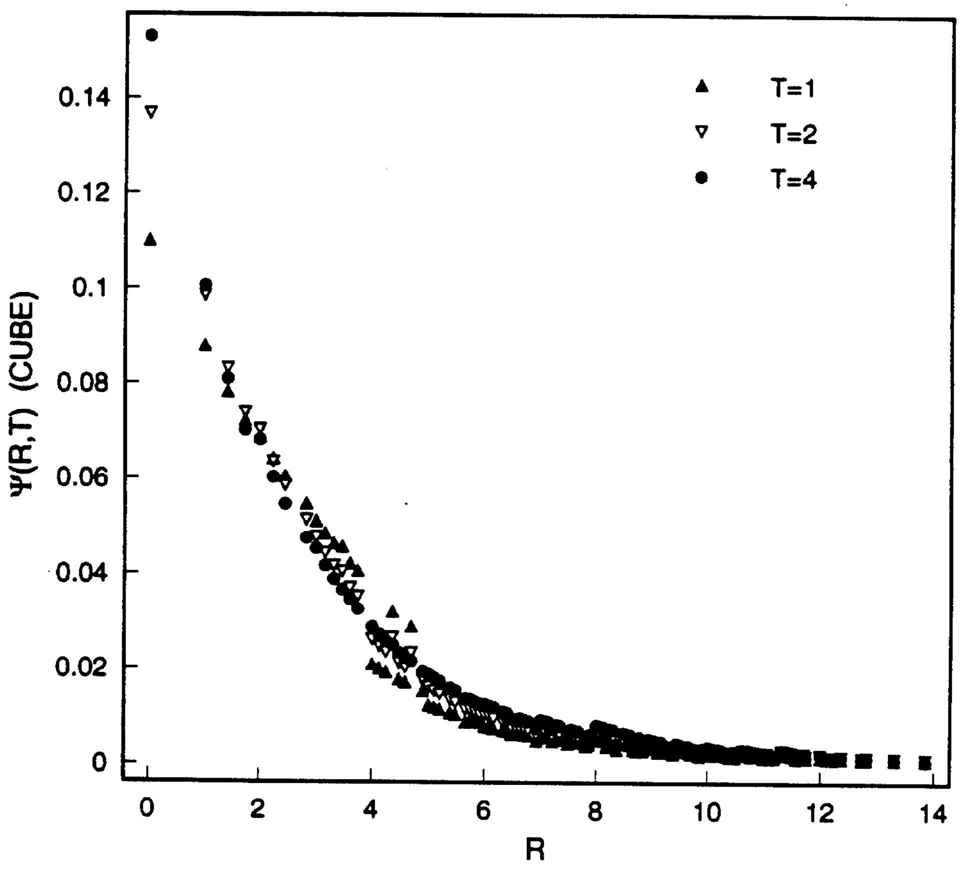

Figure 23: Time evolution of the ground state heavy-light wavefunction for $\beta = 5.9, \kappa = .159$, using a source smeared over a cube of width 7 lattice spacings

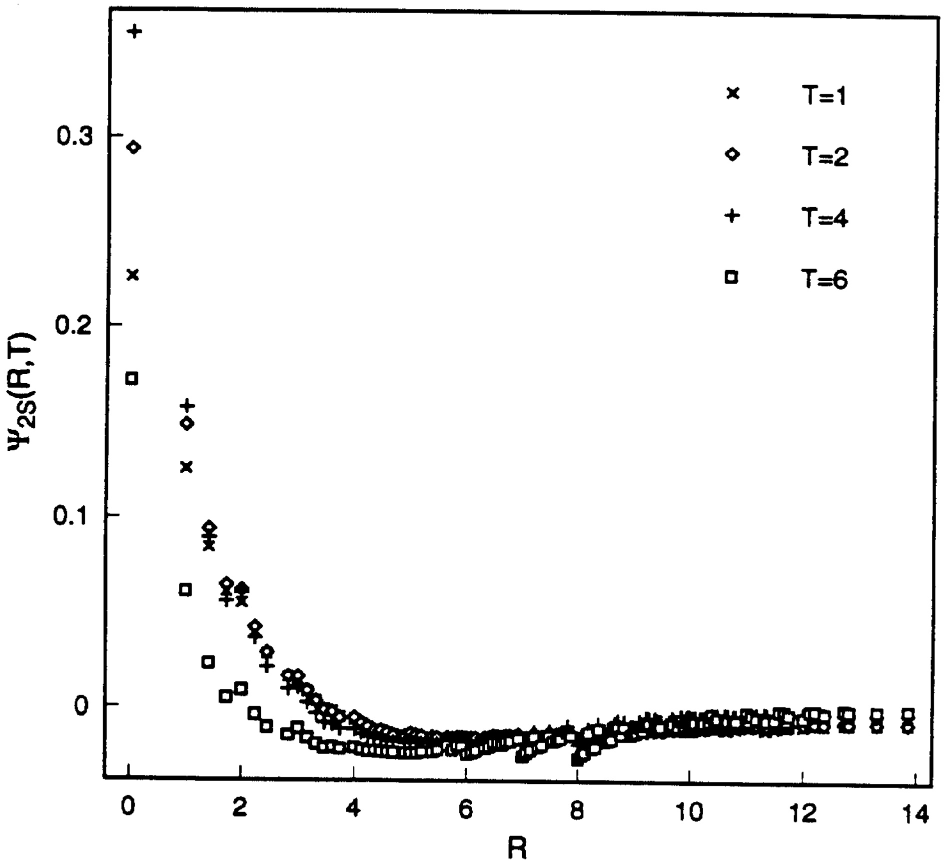

Figure 24: Time evolution of the first excited state (2S) state heavy-light wavefunction for $\beta = 5.9, \kappa = .159$, using a source smeared over the 2S RQM wavefunction.

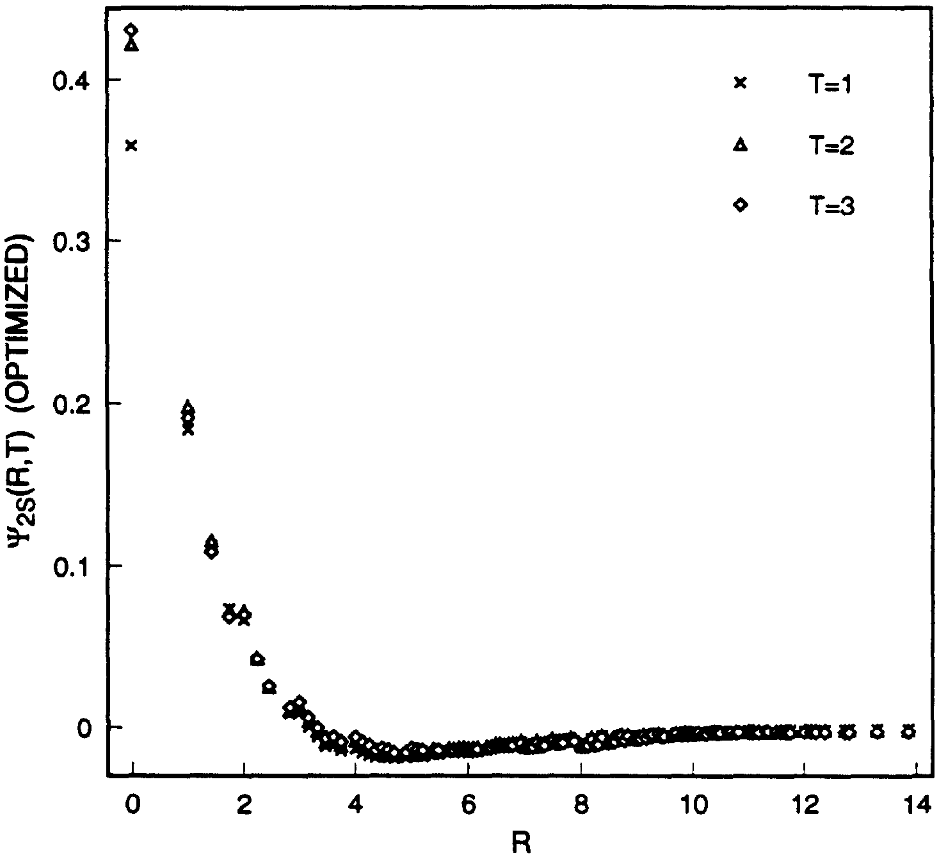

Figure 25: Time evolution of the first excited (2S) state wavefunction using a 3-state fit and selecting the optimized combination of RQM smearing functions tuned to be orthogonal to the ground state and second excited state. a Bethe-Salpeter wavefunction and optimized smearing

References

[1] E. Eichten and F. Feinberg, Phys. Rev. D **23** (1981) 2724. W. E. Caswell and G. P. Lepage, Phys. Lett. **234B** (1986) 437. E. Eichten, in Field Theory on the Lattice, Nucl. Phys. B (Proc. Suppl.) **4** (1988) 170. G. P. Lepage and B. A. Thacker, ibid. 199.

[2] A proof that these conditions are satisfied for physical systems with one heavy quark has been given in leading order in $1/m_Q$ to all orders in the loop expansion by B. Grinstein, Nucl. Phys. **B339** (1990) 253.

[3] E. Eichten and B. Hill, Phys. Lett. **234B** (1990) 511.

[4] H. Georgi, Phys. Lett. **240B** (1990) 447.

[5] N. Isgur and M. B. Wise, Phys. Lett **232B** (1989) 113; Phys. Lett **237B** (1990) 527.

[6] A. F. Falk, H. Georgi, B. Grinstein and M. B. Wise, Nucl. Phys. **B343** (1990) 1.

[7] M. B. Wise, Proceedings of the 1991 Lake Louise Winter Institute, p. 222. 1991(QCD161:L25:1991).

[8] J. D. Bjorken, SLAC preprint SLAC-PUB-5278 (1990).

[9] G.P. Lepage and B.A. Thacker, Phy. Rev D **43** (1991) 196.

[10] J. Mandula and M. Ogilvie, Nucl. Phys. (Proc. Suppl.) **26** (1992) 459; Phys. Rev. D (Rap. Comm.)**45** (1992) R2183.

[11] A. X. El-Khadra, A. S. Kronfeld, and P. B. Mackenzie, FERMILAB-PUB-93/195-T.

[12] C. W. Bernard, J. N. Labrenz, and A. Soni, Phys. Rev. D**49** (1994) 2536.

[13] A. Bartolini et al, Nucl. Phys. B (Proc.Suppl.)**30** (1993).

[14] C. Alexandrou, S. Gusken, F. Jegerlehner, K. Schilling, and R. Sommer, CERN-TH 6692/92.

[15] C. Bernard, C. M. Heard, J. Labrenz and A. Soni, Nucl. Phys. B (Proc. Suppl.) **26**, 384 (1992).

[16] A. Duncan, E. Eichten, G. Hockney, and H. Thacker, Nucl. Phys. B (Proc. Suppl.) **26**, 391 (1992).

[17] A. Duncan, E. Eichten, and H. Thacker, Phys. Lett. **B303** (1993) 109.

[18] C R Allton et al, Phys. Lett. **B326** (1994) 295.

[19] R M Baxter et al, Phys. Rev. **D49** (1994) 1594.

[20] G. P. Lepage and P. B. Mackenzie, Phys. Rev. D **48** (1993) 2250.

[21] C. Bernard, Nucl. Phys. B (Proc. Suppl.) **34** (1994) 47.

[22] O. F. Hernández and B. R. Hill, Phys. Rev. **D50** (1994) 495.

[23] S Narison, Phys Rep **84** (1982) 263 and Phys Lett B **197** (1987) 405; E Bagan et al, Phys Lett B **278** (1992) 457

[24] Particle Data Group, Phys Rev **D45** (1992) S1

[25] C A Dominguez and N Paver, Phys Lett B **293** (1992) 197; The NRQCD Collaboration, Nucl. Phys. B (Proc. Suppl.)**34** (1994) 417.

[26] M B Voloshin and M A Shifman, Yad Fiz **45** (1987) 463 [Sov J Nucl Phys **45** (1987) 292]; H D Politzer and M B Wise, Phys Lett B **206** (1988) 681 and Phys Lett B **208** (1988) 504

[27] X Ji and M J Musolf, Physics Letters B **257** (1991) 409

[28] A. Duncan, E. Eichten, J.M. Flynn, B.R. Hill, and H. Thacker, Nucl. Phys. B (Proc. Suppl.) **34**, **444** (1994).

[29] D J Broadhurst and A G Grozin, Phys Lett B **267** (1991) 105.

[30] D. J Broadhurst and A G Grozin, Phys Lett B **274** (1992) 421.

[31] E. Eichten and B. Hill, Phys Lett B **234** (1990) 511.

[32] A.F. Falk, M. Neubert, M. Luke Nucl.Phys. B **388**(1992)363.

[33] I.I. Bigi, M.A. Shifman, N.G. Uraltsev, and A.I. Vainshtein, "The Pole Mass of the Heavy Quark. Perturbation Theory and Beyond," hep-ph@xxx.lanl.gov - 9402360.

[34] E. Eichten and B. R. Hill, Phys. Lett. B **240** (1990) 193.

[35] A. Borrelli and C. Pittori, Nucl. Phys. B **385** (1992) 502; O.F. Hernández and B.R. Hill, Phys. Lett. B **289** (1992) 417.

[36] E. Schnapka, "Validity of Relativistic Potential Models in Confining Theories", Univ. of Pittsburgh Master's Thesis, Aug.1993.

[37] P.Cea, P. Colangelo, L.Cosmai, and G.Nardulli, Phys. Lett. B **206** (1988) 691.

[38] S. Gottlieb, J. Kuti, D. Touissaint, A. Kennedy, S. Meyer, B. Pendelton, and R. Sugar, Phys. Rev. Lett. **55** (1985) 1958; N. Christ and A. Terrano, Phys. Rev. Lett **56** (1985) 111.

[39] G. S. Bali and K. Schilling, Phys. Rev. D**47**, 661 (1993).

[40] D. Weingarten, Nucl. Phys.**B34** (Proc. Suppl.), 29 (1994).

[41] C. R. Allton, et al, Nucl Phys B **413** (1994) 461.

[42] Ph. Boucaud, C. L. Lin, and O. Pene, Phys. Rev. D**40**, 1529 (1989) and Phys. Rev. D**41**, 3541 (1990)(E).

[43] A. X. El-Khadra, G. M. Hockney, A. S. Kronfeld, and P. B. Mackenzie, Phys.Rev.Lett. **69** (1992) 729.

[44] C R Allton et al, Nucl Phys B **349** (1991) 349

[45] M. Luscher, in Progress in Gauge Field Theory, G. 'tHooft, et al. (eds.)(Cargese, 1983). New York:Plenum 1984.

[46] D. Hochberg and H. B. Thacker, Nucl. Phys. **B257**[FS14], (1985) 729.

[47] M. Luscher, Comm. Math. Phys. **104** (1986) 177.

[48] M. Fukugita, H. Mino, M. Okawa, G. Parisi, and A. Ukawa, Phys. Lett. **B294** (1992) 380.

[49] T Draper and C McNeile, Nucl. Phys. B (Proc. Suppl.) **34** (1994) 453.

[50] S. Hashimoto and Y. Saeki, Mod. Phys. Lett. A7, 387 (1992).